Article

Dynamical Study of Coupled Riemann Wave Equation Involving Conformable, Beta, and M-Truncated Derivatives via Two Efficient Analytical Methods

Rimsha Ansar [1], Muhammad Abbas [1,*], Pshtiwan Othman Mohammed [2,*], Eman Al-Sarairah [3,4], Khaled A. Gepreel [5] and Mohamed S. Soliman [6,*]

1   Department of Mathematics, University of Sargodha, Sargodha 40100, Pakistan
2   Department of Mathematics, College of Education, University of Sulaimani, Sulaimani 46001, Iraq
3   Department of Mathematics, Khalifa University, Abu Dhabi P.O. Box 127788, United Arab Emirates
4   Department of Mathematics, Al-Hussein Bin Talal University, P.O. Box 20, Ma'an 71111, Jordan
5   Department of Mathematics and Statistics, College of Science, Taif University, P.O. Box 11099, Taif 21944, Saudi Arabia
6   Department of Electrical Engineering, College of Engineering, Taif University, P.O. Box 11099, Taif 21944, Saudi Arabia
*   Correspondence: muhammad.abbas@uos.edu.pk (M.A.); pshtiwansangawi@gmail.com (P.O.M.); soliman@tu.edu.sa (M.S.S.)

Abstract: In this study, the Jacobi elliptic function method (JEFM) and modified auxiliary equation method (MAEM) are used to investigate the solitary wave solutions of the nonlinear coupled Riemann wave (RW) equation. Nonlinear coupled partial differential equations (NLPDEs) can be transformed into a collection of algebraic equations by utilising a travelling wave transformation. This study's objective is to learn more about the non-linear coupled RW equation, which accounts for tidal waves, tsunamis, and static uniform media. The variance in the governing model's travelling wave behavior is investigated using the conformable, beta, and M-truncated derivatives (M-TD). The aforementioned methods can be used to derive solitary wave solutions for trigonometric, hyperbolic, and jacobi functions. We may produce periodic solutions, bell-form soliton, anti-bell-shape soliton, M-shaped, and W-shaped solitons by altering specific parameter values. The mathematical form of each pair of travelling wave solutions is symmetric. Lastly, in order to emphasise the impact of conformable, beta, and M-TD on the behaviour and symmetric solutions for the presented problem, the 2D and 3D representations of the analytical soliton solutions can be produced using Mathematica 10.

Keywords: coupled Riemann wave equation; modified auxiliary equation method; Jacobi elliptic function method; beta-derivative (β-D); M-truncated derivative; conformable derivative

MSC: 39A12; 39B62; 33B10; 26A48; 26A51

1. Introduction

The nonlinear evolution equation [1,2] ia a particular class of partial differential equations (PDEs) [3]. In several branches of physical sciences, such as mathematics, notably pure and applied mathematics, biology, physics, microbiology, biochemistry, and many other subjects, these equations are widely employed as models to explain their physical significance. Nonlinear differential equations (NLDEs) are used in a wide variety of fields to describe the motion of isolated waves that are localised in a small area of space, such as physics, where they are used to study the dynamics of magneto fluids, water surface gravity waves [4], electromagnetic radiation reactions, and ion acoustic waves in plasmas [5], among many other fields. The investigation of solitary wave solutions to NLEEs [1] has become the most interesting topic for investigators as a result of the complicated behavior of NLEEs.

Similar to how fractional exponents are an extension of exponents with integer value, fractional calculus (FC) [6,7] is a branch of mathematics that developed from the usual definitions of integral and derivative operators in calculus. It is demonstrated that the physical interpretation of fractional integration is "Shadows of the past" and the geometric meaning of fractional integration is "Shadows on the walls". The initial concept of fractional differential equations (FDEs) [8] was presented in 1695 by Leibniz and L'Hopital. Applications of differential equations [9] in daily life include calculating the flow of electricity, the pendulum-like motion of an object, and deriving the principles of thermodynamics. Additionally, they are employed in medicine to graphically monitor the progression of illnesses.

Numerous definitions of the fractional-order derivative, such as the Caputo derivative (CD) [10], Grunwald–Letnikov (G-LD) [11], truncated M-fractional derivative (M-FD) [12], and an Atangana–Baleanu derivative (A-BD) [13] in the framework of Caputo, have been explored for their importance. This research considered three major fractional derivatives, namely the β-D [14], M-TD [15], and C-D [16], in order to examine the efficient solutions of the RW equation.

Models of NLPDEs from physics and mathematics serve as essentials in theoretical sciences. Numerous practical fields, including meteorology, oceanography, and the aerospace industry, depend on a grasp of these nonlinear partial differential equations. The most fundamental frameworks for analyzing nonlinear processes are nonlinear partial differential equations. A nonlinear equation known as the RW equation [17–20] is employed in the analysis of tsunami and tidal waves in oceans and rivers, stationary and uniform media, coastal and marine engineering, and in many other fields. Solitons are a prevalent class of weakly nonlinear dispersive PDEs that describe physical systems. Solitons are the solutions to these PDEs. Solitons are solitary waves with elastic dispersion characteristics; even when they collide, they maintain their shape and speed. Waves are the primary source of energy in the geographical fields involving the ecological processes brought on by transportation systems on floating or synthetic structure fields. Using the precise solutions provided by the trigonometry solution, mixed hyperbolic solution, singular solution, and periodic solution [21], the solitary patterns of the RW equation were adequately depicted. In order to investigate the effects of fractional parameters on the dynamic response of soliton waves in a non-linear coupled time-fractional RW equation, the RW equation was transformed into an ordinary differential equation using complex wave transformations for three different fractional operators, each of which provides a nonlinear algebraic equation system when the technique is applied. This leads to the presentation of certain analytically precise soliton solutions [22] derived from these equations.

In this study, the nonlinear coupled RW equation was used for analytical solutions as:

$$
\begin{aligned}
R_t + hR_{yyz} + qRE_y + rER_y &= 0, \\
R_z &= E_y,
\end{aligned}
\tag{1}
$$

where the parameters h, q, and r are non-zero. Equation (1) describes the $(2 + 1)$-dimensional interaction between a long wave propagating and a Riemann moving wave. These fully integrable equations have numerous applications in the propagation of tidal waves and ocean tsunamis. Equation (1) also includes a significant feature that combines whistling wave packets with random phases and small amplitudes to characterise the turbulent state. The magnetic sound wave faces interference caused by Whistler turbulence, which dampens it and, as a result, the electrostatic wave in the plasma.

In β-D, the proposed model takes the following form.

$$
\begin{aligned}
D_{\beta,t}^{\delta} R + hR_{yyz} + qRE_y + rER_y &= 0, \\
R_z &= E_y,
\end{aligned}
\tag{2}
$$

where $D_{\beta,t}^{\delta}$ is β-D with δ is a fractional parameter.

In M-TD, the proposed model takes the following form

$$D_{M,t}^{\delta} R + hR_{yyz} + qRE_y + rER_y = 0,$$
$$R_z = E_y,$$

(3)

where $D_{M,t}^{\delta}$ is M-TD with δ is a fractional parameter.

In C-D, the proposed model takes the following form

$$D_{c,t}^{\delta} R + hR_{yyz} + qRE_y + rER_y = 0,$$
$$R_z = E_y,$$

(4)

where $D_{c,t}^{\delta}$ and δ are called C-D and fractional parameter, respectively.

Within the computational modelling community, the idea of memory effect has long been challenging. Naturally, this memory cannot be incorporated into the traditional models [23–25]. Numerous researchers believe that fractional derivatives [26–28] can adequately explain the memory phenomenon. Khalil, et al. developed a novel concept of a derivative termed a "conformable derivative" [29]; this modified version met several established criteria, such as the chain rule. Some new properties of conformable derivative have been studied in [30,31]. The β-D is a modified conformable fractional derivative. The fractional "β-derivative" [32] was initially introduced by Atangana, et al. [33]. It also satisfies the product rule, power rule, and mean value theorem (MVT) [34]. The proposed version satisfies a number of criteria that served as restrictions on fractional derivatives and has been applied to the modelling of a number of physical issues. These derivatives can be thought of as a natural extension of the classical derivative rather than fractional derivatives. By changing the value of the fractional parameter we can observe the change in the wave profile.

A single-parameter Mittag–Leffler function [35] that also fulfills the criteria of integer-order calculus is used in an M-FD that Sousa and Oliveira introduced in 2017. This is why we are going to provide a truncated M-FD type that combines the various fractional derivative types already in existence and also meets the classical properties of integer-order calculus. Finding soliton solutions [36] for the given model with local derivatives is the aim of the research. The conformable fractional derivative (CF-D), which tries to increase the conventional derivative while meeting some natural features, provides a novel solution for different FDEs. Although exact methods are quite helpful for creating different kinds of travelling wave solutions, numerical and analytical approximate methods are more useful when finding a specific solution in cases where the initial condition can be estimated to correspond to a physical system, although many of the NLEEs still cannot be solved using the current exact solution techniques. The NLEEs have stable solutions, known as soliton solutions, in which nonlinearity and dispersion are perfectly balanced.

For the purpose of creating the doubly periodic wave solutions for special-type nonlinear equations, JEFM [37–40] with symbolic computing was developed. The effective and powerful JEFM was used to create a periodic solution for the given model. By substituting various Jacobi elliptic functions (JEF) for the tanh function, the basic notion of this technique is comparable to the tanh method. The elliptic jacobi snoidal and cnoidal functions [41], sn and cn, respectively, are used to define the sn- and cn-function approaches to finding nonsingular periodic-wave solutions to NLEEs [42] in a manner that can be automated. The solitary wave solutions of the coupled KdV equations were discovered in [43] using the homogeneous balancing approach. Lie symmetry analysis, specific solutions, and conservation laws have all been demonstrated for several partial differential equations in [44,45].

The MAEM [46–49] is a novel method for precisely solving differential equations. In this way, the auxiliary equation technique was broadened. It provides a straightforward approach to dealing with NLE solutions. This excellent strategy has been utilized to generate discoveries that are appealing and assist in the exploration of solutions to

several challenges that are developing in applied mathematics and physics. Since one may receive explicit solutions without integrating them, the approaches are appealing and effective. When using the current techniques, finding precise unique solutions is frequently challenging and, at times, impossible. Therefore, analytical approximations of solutions are obtained with the appropriate precision. These solutions could reveal additional information about the physical components of the problems as they might explain a variety of physics and other science-based phenomena, such as solitons and propagation at a finite speed. The fractional-order model [50] provide smore accurate outcomes when compared to the classical approach. Soliton solutions of fractional-order equations such as the thin-film ferroelectric material equation [50], the Fokas equation [51], and many more can also be found using MAEM.

The paper is organised as follows: Some derivative definitions and their characteristics are explained in Section 2. The mathematical analysis of the RW equation is shown in Section 3. The JEFM and MAEM analytical steps are carried out and applied to the proposed model in the Section 4. In Section 5, graphs are used in addition to computations to demonstrate how the results can be explained physically. A few closing remarks are provided in Section 6 to wrap up the study.

2. Preliminaries

Some definitions of derivatives and their basic characteristics are listed in this section.

2.1. Beta-Derivative

Definition 1. *The β-D is another kind of C-D that can be stated as [14]*

$$D_{\beta,t}^{\delta}f(t) = \lim_{\varepsilon \to 0} \frac{f(t + \varepsilon(t + \frac{1}{\Gamma(\delta)})^{1-\delta}) - f(t)}{\varepsilon}, \quad 0 < \delta \le 1.$$

The β-D possesses the following characteristics.

1. The β-D is a linear operator; that is,

$$D_{\beta,w}^{\delta}(hj(w) + kl(w)) = hD_{\beta,w}^{\delta}j(w) + kD_{\beta,w}^{\delta}l(w), \quad \forall h, \ k \in \Re.$$

2. This satisfies the product rule; that is,

$$D_{\beta,w}^{\delta}(j(w) * l(w)) = l(w)D_{\beta,w}^{\delta}j(w) + j(w)D_{\beta,w}^{\delta}l(w).$$

3. This obeys the quotient rule; that is,

$$D_{\beta,w}^{\delta}\left\{\frac{j(w)}{l(w)}\right\} = \frac{l(w)D_{\beta,w}^{\delta}j(w) - j(w)D_{\beta,w}^{\delta}l(w)}{l^2(w)}.$$

4. The β-D of a constant is zero; that is,

$$D_{\beta,w}^{\delta}(c) = 0,$$

for any constant c.

2.2. M-Truncated Derivative

Definition 2. *The M-TD for the function $f : [0, \infty) \to R$ of the order $\delta \in (0, 1)$ is defined, as [15]*

$$D_{M,t}^{\delta}f(t) = \lim_{\varepsilon \to 0} \frac{f(t \ _jE_\chi(\varepsilon t^{-\delta})) - f(t)}{\varepsilon}, \tag{5}$$

for $t > 0$, where $_jE_\chi(.), \chi > 0$ is a truncated Mittag–Leffler function of one parameter, defined as:

$$_jE_\chi(t) = \sum_{m=0}^{j} \frac{t^m}{\Gamma(\chi m + 1)}. \tag{6}$$

Theorem 1. *Let $0 < \delta \leq 1, \chi > 0$, $h, k \in R$ and j, l be δ-differentiable at a point $w > 0$. Then, [52],*

1. $D_{M,w}^{\delta}(hj(w) + kl(w)) = hD_{M,w}^{\delta}j(w) + kD_{M,w}^{\delta}l(w), \ \forall h, k \in \Re.$
2. $D_{M,w}^{\delta}(j(w) * l(w)) = l(w) \, D_{M,w}^{\delta}j(w) + j(w) \, D_{M,w}^{\delta}l(w).$
3. $D_{M,w}^{\delta}\left\{\frac{j(w)}{l(w)}\right\} = \frac{l(w)D_{M,w}^{\delta}j(w) - j(w) \, D_{M,w}^{\delta}l(w)}{l^2(w)}.$
4. *The M-TD for a differentiable function $j(w)$ is defined as:*
    $D_{M,w}^{\delta}j(w) = \frac{w^{1-\delta}}{\Gamma(\chi+1)} \frac{dj}{dw}.$

2.3. Conformable Derivative

Definition 3. *The C-D of order δ of a function $f(t)$ for a function $f : [0, \infty) \to \Re$ is written as [53]:*

$$D_{c,t}^{\delta}f(t) = \lim_{\varepsilon \to 0} \frac{f(t + \varepsilon(t)^{1-\delta}) - f(t)}{\varepsilon}, \quad \forall t > 0.$$

If e has δ-differentiability in any interval $(0, g)$ with $g > 0$, then

$$D_{c,t}^{\delta}(f(0)) = \lim_{t \to 0^+} D_{c,t}^{\delta}(f(t)),$$

whenever the limit of the right hand side exists.

Moreover, C-D-related properties and theorems are covered in [54].

3. Mathematical Analyses of the Procedure

The following transformations can be utilized to obtain soliton solutions of Equation (1)

$$R(y, z, t) = R(\varpi), \quad E(y, z, t) = E(\varpi). \tag{7}$$

The travelling wave parameter ϖ is defined in three ways.

For β-D, ϖ has the following form

$$\varpi = \mu y + \sigma z - \frac{v}{\delta}\left(t + \frac{1}{\Gamma(\delta)}\right)^{\delta}. \tag{8}$$

For M-TD, ϖ has the following form

$$\varpi = \mu y + \sigma z - v\frac{\Gamma(\chi+1)}{\delta}t^{\delta}. \tag{9}$$

For C-D, ϖ has the following form

$$\varpi = \mu y + \sigma z - \frac{v}{\delta}t^{\delta}, \tag{10}$$

where μ, σ and, v are arbitrary constants with μ, σ and, $v \neq 0$. Utilizing the transformations of Equation (7), together with Equations (8)–(10), we have

$$\begin{aligned} -vR' + h\mu^2\sigma R''' + qR\mu E' + rE\mu R' &= 0, \\ \sigma R' &= \mu E'. \end{aligned} \tag{11}$$

Using the zero integration constant to integrate the second equation of system (11), we have

$$E = \frac{\sigma}{\mu}R. \tag{12}$$

Substituting Equation (12) into the first equation of system (11) after integration, we can obtain

$$-2vR + 2h\mu^2\sigma R'' + R^2\sigma(q+r) = 0, \tag{13}$$

where $R' = \frac{dR}{d\omega}$.

4. Application of Analytical Methods

4.1. Jacobi Elliptic Function Method

Using the JEFM, $R(\omega)$ can be expressed as a finite series of Jacobi elliptical function [51], $K(\omega) = sn(\omega, m)$ for $0 < m < 1$, i.e.,

$$R(\omega) = \sum_{i=0}^{k} Psn^i(\omega, m), \tag{14}$$

the traveling wave solution for balancing principal $k = 2$ can be written as

$$R(\omega) = P_0 + P_1 K(\omega) + P_2(K(\omega))^2, \tag{15}$$

where the constants P_0, P_1, P_2 will be found later.

Substituting Equation (15) into Equation (13) yields

$$-2v(P_0 + K(\omega)(P_1 + K(\omega)P_2)) + (q+r)\sigma(P_0 + K(\omega)(P_1 + K(\omega)P_2))^2$$
$$+2h\mu^2\sigma\left(2P_2 + 6m^2K(\omega)^4P_2 + K(\omega)P_1\left(-1 - m^2 + 2m^2K(\omega)^2 - 4\left(1 + m^2\right)K(\omega)P_2\right)\right) = 0.$$

Equating each coefficient of $K(\omega)^h (h = 0, 1, 2, 3, 4)$ to zero, we have

$$-2vP_0 + q\sigma P_0^2 + r\sigma P_0^2 + 4h\mu^2\sigma P_2 = 0,$$
$$-2\left(v + h\left(1 + m^2\right)\mu^2\sigma - (q+r)\sigma P_0\right)P_1 = 0,$$
$$(q+r)\sigma P_1^2 - 2vP_2 + 2\sigma\left((q+r)P_0 - 4h\left(1 + m^2\right)\mu^2 P_1\right)P_2 = 0, \tag{16}$$
$$2\sigma P_1\left(2hm^2\mu^2 + (q+r)P_2\right) = 0,$$
$$\sigma P_2\left(12hm^2\mu^2 + (q+r)P_2\right) = 0.$$

When Equation (16) is solved, the following outcomes are obtained.

Set 1.
$$P_0 = \frac{v}{(q+r)\sigma}, P_1 = 0, P_2 = -\frac{12hm^2\mu^2}{q+r}.$$

$$R_{1,1}(y, z, t) = \frac{v}{(q+r)\sigma} - \frac{12hm^2\mu^2 sn^2(\omega, m)}{q+r}. \tag{17}$$

$$E_{1,1}(y, z, t) = \frac{\sigma\left(\frac{v}{(q+r)\sigma} - \frac{12hm^2\mu^2 sn^2(\omega, m)}{q+r}\right)}{\mu}. \tag{18}$$

If m→ 1, then Equations (17) and (18) become

$$R_{1,1}(y, z, t) = \frac{v}{(q+r)\sigma} - \frac{12h\mu^2 \tanh^2(\omega)}{q+r},$$

$$E_{1,1}(y,z,t) = \frac{\sigma\left(\frac{v}{(q+r)\sigma} - \frac{12h\mu^2\tanh^2(\varpi)}{q+r}\right)}{\mu}.$$

Set 2.

$$P_0 = \frac{-2qv - 2rv + \sqrt{(2qv + 2rv)^2 - 192h^2m^2\mu^4\sigma(-q^2\sigma - 2qr\sigma - r^2\sigma)}}{2(-q^2\sigma - 2qr\sigma - r^2\sigma)}, P_1 = 0, P_2 = -\frac{12hm^2\mu^2}{q+r}.$$

$$R_{2,1}(y,z,t) = \frac{-2qv - 2rv + \sqrt{(2qv + 2rv)^2 - 192h^2m^2\mu^4\sigma(-q^2\sigma - 2qr\sigma - r^2\sigma)}}{2(-q^2\sigma - 2qr\sigma - r^2\sigma)} \tag{19}$$
$$- \frac{12hm^2\mu^2 sn^2(\varpi, m)}{q+r}.$$

$$E_{2,1}(y,z,t) = \frac{\sigma\left(\frac{-2qv-2rv+\sqrt{(2qv+2rv)^2-192h^2m^2\mu^4\sigma(-q^2\sigma-2qr\sigma-r^2\sigma)}}{2(-q^2\sigma-2qr\sigma-r^2\sigma)} - \frac{12hm^2\mu^2 sn^2(\varpi,m)}{q+r}\right)}{\mu}. \tag{20}$$

If m→ 1, then Equation (19) and Equation (20) become

$$R_{2,1}(y,z,t) = \frac{-2qv - 2rv + \sqrt{(2qv + 2rv)^2 - 192h^2\mu^4\sigma(-q^2\sigma - 2qr\sigma - r^2\sigma)}}{2(-q^2\sigma - 2qr\sigma - r^2\sigma)} - \frac{12h\mu^2\tanh^2(\varpi)}{q+r},$$

$$E_{2,1}(y,z,t) = \frac{\sigma\left(\frac{-2qv-2rv+\sqrt{(2qv+2rv)^2-192h^2\mu^4\sigma(-q^2\sigma-2qr\sigma-r^2\sigma)}}{2(-q^2\sigma-2qr\sigma-r^2\sigma)} - \frac{12h\mu^2\tanh^2(\varpi)}{q+r}\right)}{\mu}.$$

Set 3.

$$P_0 = \frac{2qv + 2rv + \sqrt{(2qv + 2rv)^2 - 192h^2m^2\mu^4\sigma(-q^2\sigma - 2qr\sigma - r^2\sigma)}}{2(q^2\sigma + 2qr\sigma + r^2\sigma)}, P_1 = 0, P_2 = -\frac{12hm^2\mu^2}{q+r}.$$

$$R_{3,1}(y,z,t) = \frac{2qv + 2rv + \sqrt{(2qv + 2rv)^2 - 192h^2m^2\mu^4\sigma(-q^2\sigma - 2qr\sigma - r^2\sigma)}}{2(q^2\sigma + 2qr\sigma + r^2\sigma)} \tag{21}$$
$$- \frac{12hm^2\mu^2 sn^2(\varpi, m)}{q+r}.$$

$$E_{3,1}(y,z,t) = \frac{\sigma\left(\frac{2qv+2rv+\sqrt{(2qv+2rv)^2-192h^2m^2\mu^4\sigma(-q^2\sigma-2qr\sigma-r^2\sigma)}}{2(q^2\sigma+2qr\sigma+r^2\sigma)} - \frac{12hm^2\mu^2 sn^2(\varpi,m)}{q+r}\right)}{\mu}. \tag{22}$$

If m→ 1, then Equation (21) and Equation (22) become

$$R_{3,1}(y,z,t) = \frac{2qv + 2rv + \sqrt{(2qv + 2rv)^2 - 192h^2\mu^4\sigma(-q^2\sigma - 2qr\sigma - r^2\sigma)}}{2(q^2\sigma + 2qr\sigma + r^2\sigma)} - \frac{12h\mu^2\tanh^2(\varpi)}{q+r},$$

$$E_{3,1}(y,z,t) = \frac{\sigma\left(\frac{2qv+2rv+\sqrt{(2qv+2rv)^2-192h^2\mu^4\sigma(-q^2\sigma-2qr\sigma-r^2\sigma)}}{2(q^2\sigma+2qr\sigma+r^2\sigma)} - \frac{12h\mu^2\tanh^2(\varpi)}{q+r}\right)}{\mu}.$$

Analogously, we can replace $\text{sn}(\omega, m)$ with $\text{cn}(\omega, m)$ and $\text{dn}(\omega, m)$ to obtain solutions to Equation (13).

4.2. Modified Auxiliary Equation Method

In order to obtain the traveling wave solutions, the MAEM [46] offers the general solution in the form

$$R(\omega) = P_0 + \sum_{h=1}^{j} \left[P_h(\zeta^u)^h + Q_h(\zeta^u)^{-h} \right], \tag{23}$$

where P_0, P_h's and Q_h's are unknown constants. In the auxiliary equation, the function is stated $u(\omega)$.

$$\ln(\zeta) * u'(\omega) = d + x\zeta^{-u} + w\zeta^u, \tag{24}$$

for arbitrary constant values of d, x and w ($\zeta > 0, \zeta \neq 1$).
Here, cases for Equation (24) are discussed.

1. If $d^2 - 4xw < 0$ *and* $w \neq 0$, then

$$2w * \zeta^{u(\omega)} = -d + \sqrt{4xw - d^2} \tan\left(\frac{\sqrt{4xw - d^2}\omega}{2} \right), \tag{25}$$

   or

$$2w * \zeta^{u(\omega)} = -(d + \sqrt{4xw - d^2}\cot\left(\frac{\sqrt{4xw - d^2}\omega}{2} \right)). \tag{26}$$

2. If $d^2 - 4xw > 0$ and $w \neq 0$, then

$$2w * \zeta^{u(\omega)} = -(d + \sqrt{d^2 - 4xw} \tanh\left(\frac{\sqrt{d^2 - 4xw}\omega}{2} \right)), \tag{27}$$

   or

$$2w * \zeta^{u(\omega)} = -(d + \sqrt{d^2 - 4xw} \coth\left(\frac{\sqrt{d^2 - 4xw}\omega}{2} \right)). \tag{28}$$

3. If $d^2 - 4xw = 0$ and $w \neq 0$, then

$$\zeta^{u(\omega)} = -\frac{2 + d\omega}{2w\omega}. \tag{29}$$

In Equation (13), the highest order derivative R'' and highest order nonlinear term R^2 are balanced in accordance with the homogeneous balancing principle, resulting in $j = 2$.

$$R(\omega) = P_0 + P_1\zeta^u + Q_1\zeta^{-u} + P_2\zeta^{2u} + Q_2\zeta^{-2u}. \tag{30}$$

The set of algebraic equations produced when each coefficient of $\zeta^{u(\omega)}$ is made equal to zero is as follows:

$$\zeta^{u(\varpi)^{-4}} : \sigma Q_2\Big(12hx^2\mu^2 + (q+r)Q_2\Big) = 0,$$

$$\zeta^{u(\varpi)^{-3}} : 2\sigma\Big(10dhx\mu^2 Q_2 + Q_1\Big(2hx^2\mu^2 + (q+r)Q_2\Big)\Big) = 0,$$

$$\zeta^{u(\varpi)^{-2}} : 6dhx\mu^2\sigma Q_1 + (q+r)\sigma Q_1^2 + 2\Big(-v + 4h\Big(d^2 + 2wx\Big)\mu^2\sigma + (q+r)\sigma P_0\Big)Q_2 = 0,$$

$$\zeta^{u(\varpi)^{-1}} : 2\Big(\Big(-v + h\Big(d^2 + 2wx\Big)\mu^2\sigma + (q+r)\sigma P_0\Big)Q_1 + \sigma\Big(6dhw\mu^2 + (q+r)P_1\Big)Q_2\Big) = 0,$$

$$\zeta^{u(\varpi)^{0}} : -2vP_0 + q\sigma P_0^2 + r\sigma P_0^2 + 2dhx\mu^2\sigma P_1 + 4hx^2\mu^2\sigma P_2 + 2dhw\mu^2\sigma Q_1 + $$
$$2q\sigma P_1 Q_1 + 2r\sigma P_1 Q_1 + 2q\sigma P_2 Q_2 + 2r\sigma P_2 Q_2 = 0,$$

$$\zeta^{u(\varpi)^{1}} : 2\Big(\Big(-v + h\Big(d^2 + 2wx\Big)\mu^2\sigma + (q+r)\sigma P_0\Big)P_1 + \sigma P_2\Big(6dhx\mu^2 + (q+r)Q_1\Big)\Big) = 0,$$

$$\zeta^{u(\varpi)^{2}} : 6dhw\mu^2\sigma P_1 + (q+r)\sigma P_1^2 + 2\Big(-v + 4h\Big(d^2 + 2wx\Big)\mu^2\sigma + (q+r)\sigma P_0\Big)P_2 = 0,$$

$$\zeta^{u(\varpi)^{3}} : 2\sigma\Big(10dhw\mu^2 P_2 + P_1\Big(2hw^2\mu^2 + (q+r)P_2\Big)\Big) = 0,$$

$$\zeta^{u(\varpi)^{4}} : \sigma P_2\Big(12hw^2\mu^2 + (q+r)P_2\Big) = 0.$$

The following families are produced by solving the aforementioned equations.

Family 1: When

$$P_0 = \frac{v - d^2h\mu^2\sigma - 8hwx\mu^2\sigma}{(q+r)\sigma}, P_1 = -\frac{12dhw\mu^2}{q+r}, P_2 = -\frac{12hw^2\mu^2}{q+r}, Q_1 = 0, Q_2 = 0.$$

The following cases will occur:

- For $d^2 - 4xw < 0$ and $w \neq 0$, the trigonometric solution is:

$$R_{1,1}(y,z,t) = \frac{\begin{aligned}&vw^2 - h\big(d^2\big(3r^2 - 6rw + w^2\big) + 8rw^2x\big)\mu^2\sigma + 3hr\mu^2\sigma \tan\Big(\tfrac{1}{2}\sqrt{-d^2 + 4wx}\varpi\Big)\\ &\Big(2d(r-w)\sqrt{-d^2 + 4wx} + r\big(d^2 - 4wx\big)\tan\Big(\tfrac{1}{2}\sqrt{-d^2 + 4wx}\varpi\Big)\Big)\end{aligned}}{(q+r)w^2\sigma},$$

$$E_{1,1}(y,z,t) = \frac{\sigma\left(\begin{aligned}&\frac{v - d^2h\mu^2\sigma - 8hrx\mu^2\sigma}{(q+r)\sigma} - \frac{6dhr\mu^2\big(-d+\sqrt{-d^2+4wx}\tan\big(\tfrac{1}{2}\sqrt{-d^2+4wx}\varpi\big)\big)}{(q+r)w}\\ &-\frac{3hr^2\mu^2\big(-d+\sqrt{-d^2+4wx}\tan\big(\tfrac{1}{2}\sqrt{-d^2+4wx}\varpi\big)\big)^2}{(q+r)w^2}\end{aligned}\right)}{\mu},$$

or

$$R_{1,2}(y,z,t) = \frac{\begin{aligned}&vw^2 - h\big(d^2\big(3r^2 - 6rw + w^2\big) + 8rw^2x\big)\mu^2\sigma + 3hr\mu^2\sigma \cot\Big(\tfrac{1}{2}\sqrt{-d^2 + 4wx}\varpi\Big)\\ &\Big(2d(-r+w)\sqrt{-d^2 + 4wx} + r\big(d^2 - 4wx\big)\cot\Big(\tfrac{1}{2}\sqrt{-d^2 + 4wx}\varpi\Big)\Big)\end{aligned}}{(q+r)w^2\sigma},$$

$$E_{1,2}(y,z,t) = \frac{\sigma\left(\begin{aligned}&\frac{v - d^2h\mu^2\sigma - 8hrx\mu^2\sigma}{(q+r)\sigma} + \frac{6dhr\mu^2\big(d+\sqrt{-d^2+4wx}\cot\big(\tfrac{1}{2}\sqrt{-d^2+4wx}\varpi\big)\big)}{(q+r)w}\\ &-\frac{3hr^2\mu^2\big(d+\sqrt{-d^2+4wx}\cot\big(\tfrac{1}{2}\sqrt{-d^2+4wx}\varpi\big)\big)^2}{(q+r)w^2}\end{aligned}\right)}{\mu}.$$

- For $d^2 - 4xw > 0$ and $w \neq 0$, the hyperbolic solution is:

$$R_{1,3}(y,z,t) = \frac{\begin{aligned}&vw^2 - h\big(d^2\big(3r^2 - 6rw + w^2\big) + 8rw^2x\big)\mu^2\sigma - 3hr\mu^2\sigma \tanh\Big(\tfrac{1}{2}\sqrt{d^2 - 4wx}\varpi\Big)\\ &\Big(2d(r-w)\sqrt{d^2 - 4wx} + r\big(d^2 - 4wx\big)\tanh\Big(\tfrac{1}{2}\sqrt{d^2 - 4wx}\varpi\Big)\Big)\end{aligned}}{(q+r)w^2\sigma},$$

$$E_{1,3}(y,z,t) = \frac{\sigma\left(\begin{array}{c} \frac{v - d^2 h\mu^2\sigma - 8hrx\mu^2\sigma}{(q+r)\sigma} + \frac{6dhr\mu^2\left(d+\sqrt{d^2-4wx}\tanh\left(\frac{1}{2}\sqrt{d^2-4wx}\varpi\right)\right)}{(q+r)w} \\ -\frac{3hr^2\mu^2\left(d+\sqrt{d^2-4wx}\tanh\left(\frac{1}{2}\sqrt{d^2-4wx}\varpi\right)\right)^2}{(q+r)w^2} \end{array}\right)}{\mu},$$

or

$$R_{1,4}(y,z,t) = \frac{\begin{array}{c} vw^2 - h\left(d^2\left(3r^2 - 6rw + w^2\right) + 8rw^2 x\right)\mu^2\sigma - 3hr\mu^2\sigma\coth\left[\frac{1}{2}\sqrt{d^2-4wx}\varpi\right] \\ \left(2d(r-w)\sqrt{d^2-4wx} + r\left(d^2-4wx\right)\coth\left[\frac{1}{2}\sqrt{d^2-4wx}\varpi\right]\right) \end{array}}{(q+r)w^2\sigma},$$

$$E_{1,4}(y,z,t) = \frac{\sigma\left(\begin{array}{c} \frac{v - d^2 h\mu^2\sigma - 8hrx\mu^2\sigma}{(q+r)\sigma} + \frac{6dhr\mu^2\left(d+\sqrt{d^2-4wx}\coth\left[\frac{1}{2}\sqrt{d^2-4wx}\varpi\right]\right)}{(q+r)w} \\ -\frac{3hr^2\mu^2\left(d+\sqrt{d^2-4wx}\coth\left[\frac{1}{2}\sqrt{d^2-4wx}\varpi\right]\right)^2}{(q+r)w^2} \end{array}\right)}{\mu}.$$

Family 2: When

$$P_0 = \frac{v - d^2 h\mu^2\sigma - 8hwx\mu^2\sigma}{(q+r)\sigma}, P_1 = 0, P_2 = 0, Q_1 = -\frac{12dhx\mu^2}{q+r}, Q_2 = -\frac{12hx^2\mu^2}{q+r}.$$

The following cases will occur:

- For $d^2 - 4xw < 0$ and $w \neq 0$, the trigonometric solution is:

$$R_{2,1}(y,z,t) = \frac{\frac{v}{\sigma} + h\mu^2\left(\begin{array}{c} -d^2 + \frac{24dwx}{d - \sqrt{-d^2+4wx}\tan\left(\frac{1}{2}\sqrt{-d^2+4wx}\varpi\right)} \\ +8x\left(-r - \frac{6w^2 x}{\left(d - \sqrt{-d^2+4wx}\tan\left(\frac{1}{2}\sqrt{-d^2+4wx}\varpi\right)\right)^2}\right) \end{array}\right)}{q+r},$$

$$E_{2,1}(y,z,t) = \frac{\sigma\left(\begin{array}{c} \frac{v - d^2 h\mu^2\sigma - 8hrx\mu^2\sigma}{(q+r)\sigma} - \frac{48hw^2 x^2\mu^2}{(q+r)\left(-d+\sqrt{-d^2+4wx}\tan\left(\frac{1}{2}\sqrt{-d^2+4wx}\varpi\right)\right)^2} \\ -\frac{24dhwx\mu^2}{(q+r)\left(-d+\sqrt{-d^2+4wx}\tan\left(\frac{1}{2}\sqrt{-d^2+4wx}\varpi\right)\right)} \end{array}\right)}{\mu},$$

or

$$R_{2,2}(y,z,t) = \frac{\frac{v}{\sigma} + h\mu^2\left(\begin{array}{c} -d^2 + \frac{24dwx}{d + \sqrt{-d^2+4wx}\cot\left(\frac{1}{2}\sqrt{-d^2+4wx}\varpi\right)} \\ +8x\left(-r - \frac{6w^2 x}{\left(d + \sqrt{-d^2+4wx}\cot\left(\frac{1}{2}\sqrt{-d^2+4wx}\varpi\right)\right)^2}\right) \end{array}\right)}{q+r},$$

$$E_{2,2}(y,z,t) = \frac{\sigma\left(\begin{array}{c} \frac{v - d^2 h\mu^2\sigma - 8hrx\mu^2\sigma}{(q+r)\sigma} - \frac{48hw^2 x^2\mu^2}{(q+r)\left(d+\sqrt{-d^2+4wx}\cot\left(\frac{1}{2}\sqrt{-d^2+4wx}\varpi\right)\right)^2} \\ +\frac{24dhwx\mu^2}{(q+r)\left(d+\sqrt{-d^2+4wx}\cot\left(\frac{1}{2}\sqrt{-d^2+4wx}\varpi\right)\right)} \end{array}\right)}{\mu}.$$

- For $d^2 - 4xw > 0$ and $w \neq 0$, the hyperbolic solution is:

$$R_{2,3}(y,z,t) = \frac{\frac{v}{\sigma} + h\mu^2 \left(\begin{array}{c} -d^2 + \frac{24dwx}{d+\sqrt{d^2-4wx}\tanh\left(\frac{1}{2}\sqrt{d^2-4wx}\varpi\right)} \\ +8x\left(-r - \frac{6w^2x}{\left(d+\sqrt{d^2-4wx}\tanh\left(\frac{1}{2}\sqrt{d^2-4wx}\varpi\right)\right)^2}\right) \end{array} \right)}{q+r},$$

$$E_{2,3}(y,z,t) = \frac{\sigma\left(\begin{array}{c} \frac{v-d^2h\mu^2\sigma-8hrx\mu^2\sigma}{(q+r)\sigma} - \frac{48hw^2x^2\mu^2}{(q+r)\left(d+\sqrt{d^2-4wx}\tanh\left(\frac{1}{2}\sqrt{d^2-4wx}\varpi\right)\right)^2} \\ + \frac{24dhwx\mu^2}{(q+r)\left(d+\sqrt{d^2-4wx}\tanh\left(\frac{1}{2}\sqrt{d^2-4wx}\varpi\right)\right)} \end{array} \right)}{\mu},$$

or

$$R_{2,4}(y,z,t) = \frac{\frac{v}{\sigma} + h\mu^2 \left(\begin{array}{c} -d^2 + \frac{24dwx}{d+\sqrt{d^2-4wx}\coth\left(\frac{1}{2}\sqrt{d^2-4wx}\varpi\right)} \\ +8x\left(-r - \frac{6w^2x}{\left(d+\sqrt{d^2-4wx}\coth\left(\frac{1}{2}\sqrt{d^2-4wx}\varpi\right)\right)^2}\right) \end{array} \right)}{q+r},$$

$$E_{2,4}(y,z,t) = \frac{\sigma\left(\begin{array}{c} \frac{v-d^2h\mu^2\sigma-8hrx\mu^2\sigma}{(q+r)\sigma} - \frac{48hw^2x^2\mu^2}{(q+r)\left(d+\sqrt{d^2-4wx}\coth\left(\frac{1}{2}\sqrt{d^2-4wx}\varpi\right)\right)^2} \\ + \frac{24dhwx\mu^2}{(q+r)\left(d+\sqrt{d^2-4wx}\coth\left(\frac{1}{2}\sqrt{d^2-4wx}\varpi\right)\right)} \end{array} \right)}{\mu}.$$

Family 3: When

$$P_0 = \frac{v - d^2h\mu^2\sigma - 8hwx\mu^2\sigma}{(q+r)\sigma}, P_1 = -\frac{12dhw\mu^2}{q+r}, P_2 = -\frac{12hw^2\mu^2}{q+r},$$

$$Q_1 = -\frac{12dhx\mu^2}{q+r}, Q_2 = -\frac{12hx^2\mu^2}{q+r}.$$

The following cases will occur:

- For $d^2 - 4xw < 0$ and $w \neq 0$, the trigonometric solution is:

$$\psi = \sqrt{-d^2 + 4wx}$$

$$R_{3,1}(y,z,t) = \left(\begin{array}{c} \frac{\frac{8w^3x\left(d^2-2wx-d\psi\tan\left(\frac{1}{2}\psi\varpi\right)\right)}{\left(d-\psi\tan\left(\frac{1}{2}\psi\varpi\right)\right)^2}}{q+r} + \frac{3h\mu^2\left(2dr(r-w)\psi\tan\left(\frac{1}{2}\psi\varpi\right)+r^2\left(d^2-4wx\right)\tan\left(\frac{1}{2}\psi\varpi\right)^2\right)}{w^2}) \\ + \frac{-\frac{d^2h\left(3r^2-6rw+w^2\right)\mu^2}{w^2}-8hrx\mu^2+\frac{v}{\sigma}}{q+r} \end{array} \right),$$

$$E_{3,1}(y,z,t) = \frac{\sigma}{\mu}\left(\begin{array}{c} \frac{v-d^2h\mu^2\sigma-8hrx\mu^2\sigma}{(q+r)\sigma} - \frac{48hw^2x^2\mu^2}{(q+r)\left(-d+\psi\tan\left(\frac{1}{2}\psi\varpi\right)\right)^2} - \frac{24dhwx\mu^2}{(q+r)\left(-d+\psi\tan\left(\frac{1}{2}\psi\varpi\right)\right)} \\ - \frac{6dhr\mu^2\left(-d+\psi\tan\left(\frac{1}{2}\psi\varpi\right)\right)}{(q+r)w} - \frac{3hr^2\mu^2\left(-d+\psi\tan\left(\frac{1}{2}\psi\varpi\right)\right)^2}{(q+r)w^2} \end{array} \right),$$

or

$$R_{3,2}(y,z,t) = \left(\begin{array}{c} \frac{-\frac{d^2h\left(3r^2-6rw+w^2\right)\mu^2}{w^2}-8hrx\mu^2+\frac{v}{\sigma}}{q+r} + \frac{3h\mu^2\left(2dr(r-w)\psi\cot\left(\frac{1}{2}\psi\varpi\right)+r^2\left(d^2-4wx\right)\cot\left(\frac{1}{2}\psi\varpi\right)^2\right)}{w^2}) \\ + \frac{\frac{8w^3x\left(d^2-2wx-d\psi\cot\left(\frac{1}{2}\psi\varpi\right)\right)}{\left(d-\psi\cot\left(\frac{1}{2}\psi\varpi\right)\right)^2}}{q+r} \end{array} \right),$$

$$E_{3,2}(y,z,t) = \frac{\sigma}{\mu} \begin{pmatrix} \frac{v - d^2 h\mu^2\sigma - 8hrx\mu^2\sigma}{(q+r)\sigma} - \frac{48hw^2x^2\mu^2}{(q+r)\left(-d+\psi\cot\left(\frac{1}{2}\psi\omega\right)\right)^2} - \frac{24dhwx\mu^2}{(q+r)\left(-d+\psi\cot\left(\frac{1}{2}\psi\omega\right)\right)} \\ \\ - \frac{6dhr\mu^2\left(-d+\psi\cot\left(\frac{1}{2}\psi\omega\right)\right)}{(q+r)w} - \frac{3hr^2\mu^2\left(-d+\psi\cot\left(\frac{1}{2}\psi\omega\right)\right)^2}{(q+r)w^2} \end{pmatrix}.$$

- For $d^2 - 4xw > 0$ and $w \neq 0$, the hyperbolic solution is:

$$\psi = \sqrt{d^2 - 4wx}$$

$$R_{3,3}(y,z,t) = \frac{1}{q+r} \begin{pmatrix} -h\left(d^2+8rx\right)\mu^2 + \frac{v}{\sigma} - \frac{48hw^2x^2\mu^2}{\left(d+\psi\tanh\left(\frac{1}{2}\psi\omega\right)\right)^2} + \frac{24dhwx\mu^2}{d+\psi\tanh\left(\frac{1}{2}\psi\omega\right)} \\ \\ + \frac{6dhr\mu^2\left(d+\psi\tanh\left(\frac{1}{2}\psi\omega\right)\right)}{w} - \frac{3hr^2\mu^2\left(d+\psi\tanh\left(\frac{1}{2}\psi\omega\right)\right)^2}{w^2} \end{pmatrix},$$

$$E_{3,3}(y,z,t) = \frac{\sigma}{\mu} \begin{pmatrix} \frac{v - d^2 h\mu^2\sigma - 8hrx\mu^2\sigma}{(q+r)\sigma} - \frac{48hw^2x^2\mu^2}{(q+r)\left(d+\psi\tanh\left(\frac{1}{2}\psi\omega\right)\right)^2} + \frac{24dhwx\mu^2}{(q+r)\left(d+\psi\tanh\left(\frac{1}{2}\psi\omega\right)\right)} \\ \\ + \frac{6dhr\mu^2\left(d+v\tanh\left(\frac{1}{2}\psi\omega\right)\right)}{(q+r)w} - \frac{3hr^2\mu^2\left(d+\psi\tanh\left(\frac{1}{2}\psi\omega\right)\right)^2}{(q+r)w^2} \end{pmatrix},$$

or

$$R_{3,4}(y,z,t) = \frac{1}{q+r} \begin{pmatrix} -h\left(d^2+8rx\right)\mu^2 + \frac{v}{\sigma} - \frac{48hw^2x^2\mu^2}{\left(d+\psi\coth\left(\frac{1}{2}\psi\omega\right)\right)^2} + \frac{24dhwx\mu^2}{d+\psi\coth\left(\frac{1}{2}\psi\omega\right)} \\ \\ + \frac{6dhr\mu^2\left(d+\psi\coth\left(\frac{1}{2}\psi\omega\right)\right)}{w} - \frac{3hr^2\mu^2\left(d+\psi\coth\left(\frac{1}{2}\psi\omega\right)\right)^2}{w^2} \end{pmatrix},$$

$$E_{3,4}(y,z,t) = \frac{\sigma}{\mu} \begin{pmatrix} \frac{v - d^2 h\mu^2\sigma - 8hrx\mu^2\sigma}{(q+r)\sigma} - \frac{48hw^2x^2\mu^2}{(q+r)\left(d+\psi\coth\left(\frac{1}{2}\psi\omega\right)\right)^2} + \frac{24dhwx\mu^2}{(q+r)\left(d+\psi\coth\left(\frac{1}{2}\psi\omega\right)\right)} \\ \\ + \frac{6dhr\mu^2\left(d+v\coth\left(\frac{1}{2}\psi\omega\right)\right)}{(q+r)w} - \frac{3hr^2\mu^2\left(d+\psi\coth\left(\frac{1}{2}\psi\omega\right)\right)^2}{(q+r)w^2} \end{pmatrix}.$$

Family 4: When

$$P_0 = \frac{v - d^2 h\mu^2\sigma - 8hrwx\mu^2\sigma}{(q+r)\sigma}, P_1 = -\frac{12dhw\mu^2}{q+r}, P_2 = -\frac{12hw^2\mu^2}{q+r},$$

$$Q_1 = -\frac{4dhx\mu^2}{q+r}, Q_2 = \frac{4hx^2\mu^2}{3(q+r)}.$$

The following cases will occur:

- For $d^2 - 4xw < 0$ and $w \neq 0$, the trigonometric solution is:

$$\psi = \sqrt{-d^2 + 4wx}$$

$$R_{4,1}(y,z,t) = \frac{1}{3(q+r)} \begin{pmatrix} -\frac{3h\left(d^2\left(3r^2-6rw+w^2\right)+8rw^2x\right)\mu^2}{w^2} \\ + \frac{h\mu^2\left(18dr(r-w)\psi\tan\left(\frac{1}{2}\psi\omega\right)+9r^2\left(d^2-4wx\right)\tan\left(\frac{1}{2}\psi\omega\right)^2\right)}{w^2} \\ \frac{8w^3x\left(3d^2+2wx-3d\psi\tan\left(\frac{1}{2}\psi\omega\right)\right)}{\left(d-\psi\tan\left(\frac{1}{2}\psi\omega\right)\right)^2} \\ + \frac{}{w^2} + \frac{3v}{\sigma} \end{pmatrix},$$

$$E_{4,1}(y,z,t) = \frac{\sigma}{\mu} \begin{pmatrix} \frac{v - d^2 h\mu^2\sigma - 8hrx\mu^2\sigma}{(q+r)\sigma} + \frac{16hw^2x^2\mu^2}{3(q+r)\left(-d+\psi\tan\left(\frac{1}{2}\psi\omega\right)\right)^2} - \frac{8dhwx\mu^2}{(q+r)\left(-d+\psi\tan\left(\frac{1}{2}\psi\omega\right)\right)} \\ \\ - \frac{6dhr\mu^2\left(-d+\psi\tan\left(\frac{1}{2}\psi\omega\right)\right)}{(q+r)w} - \frac{3hr^2\mu^2\left(-d+\psi\tan\left(\frac{1}{2}\psi\omega\right)\right)^2}{(q+r)w^2} \end{pmatrix},$$

or

$$R_{4,2}(y,z,t) = \frac{1}{3(q+r)} \left(\begin{array}{c} -\dfrac{3h\left(d^2\left(3r^2-6rw+w^2\right)+8rw^2x\right)\mu^2}{w^2} \\[3mm] +\dfrac{h\mu^2(18dr(r-w)\psi}{w^2}\dfrac{\cot\left(\frac{1}{2}\psi\varpi\right)+9r^2\left(d^2-4wx\right)\cot\left(\frac{1}{2}\psi\varpi\right)^2}{w^2} \\[3mm] +\dfrac{\frac{8w^3x\left(3d^2+2wx-3d\psi\cot\left(\frac{1}{2}\psi\varpi\right)\right)}{\left(d-\psi\cot\left(\frac{1}{2}\psi\varpi\right)\right)^2}}{w^2} + \dfrac{3v}{\sigma} \end{array} \right),$$

$$E_{4,2}(y,z,t) = \frac{\sigma}{\mu} \left(\begin{array}{c} \dfrac{v-d^2h\mu^2\sigma-8hrx\mu^2\sigma}{(q+r)\sigma} + \dfrac{16hw^2x^2\mu^2}{3(q+r)\left(-d+\psi\cot\left(\frac{1}{2}\psi\varpi\right)\right)^2} - \dfrac{8dhwx\mu^2}{(q+r)\left(-d+\psi\cot\left(\frac{1}{2}\psi\varpi\right)\right)} \\[3mm] -\dfrac{6dhr\mu^2\left(-d+\psi\cot\left(\frac{1}{2}\psi\varpi\right)\right)}{(q+r)w} - \dfrac{3hr^2\mu^2\left(-d+\psi\cot\left(\frac{1}{2}\psi\varpi\right)\right)^2}{(q+r)w^2} \end{array} \right).$$

- For $d^2 - 4xw > 0$ and $w \neq 0$, the hyperbolic solution is:

$$\psi = \sqrt{d^2 - 4wx}$$

$$R_{4,3}(y,z,t) = \frac{1}{3(q+r)} \left(\begin{array}{c} -3h\left(d^2+8rx\right)\mu^2 + \dfrac{3v}{\sigma} + \dfrac{16hw^2x^2\mu^2}{\left(d+\psi\tanh\left(\frac{1}{2}\psi\varpi\right)\right)^2} + \dfrac{24dhwx\mu^2}{d+\psi\tanh\left(\frac{1}{2}\psi\varpi\right)} \\[3mm] -\dfrac{9hr^2\mu^2\left(d+\psi\tanh\left(\frac{1}{2}\psi\varpi\right)\right)^2}{w^2} + \dfrac{18dhr\mu^2\left(d+\psi\tanh\left(\frac{1}{2}\psi\varpi\right)\right)}{w} \end{array} \right),$$

$$E_{4,3}(y,z,t) = \frac{\sigma}{\mu} \left(\begin{array}{c} \dfrac{v-d^2h\mu^2\sigma-8hrx\mu^2\sigma}{(q+r)\sigma} + \dfrac{16hw^2x^2\mu^2}{3(q+r)\left(d+\psi\tanh\left(\frac{1}{2}\psi\varpi\right)\right)^2} + \dfrac{8dhwx\mu^2}{(q+r)\left(d+\psi\tanh\left(\frac{1}{2}\psi\varpi\right)\right)} \\[3mm] +\dfrac{6dhr\mu^2\left(d+\psi\tanh\left(\frac{1}{2}\psi\varpi\right)\right)}{(q+r)w} - \dfrac{3hr^2\mu^2\left(d+\psi\tanh\left(\frac{1}{2}\psi\varpi\right)\right)^2}{(q+r)w^2} \end{array} \right),$$

or

$$R_{4,4}(y,z,t) = \frac{1}{3(q+r)} \left(\begin{array}{c} -3h\left(d^2+8rx\right)\mu^2 + \dfrac{3v}{\sigma} + \dfrac{16hw^2x^2\mu^2}{\left(d+\psi\coth\left(\frac{1}{2}\psi\varpi\right)\right)^2} + \dfrac{24dhwx\mu^2}{d+\psi\coth\left(\frac{1}{2}\psi\varpi\right)} \\[3mm] -\dfrac{9hr^2\mu^2\left(d+\psi\coth\left(\frac{1}{2}\psi\varpi\right)\right)^2}{w^2} + \dfrac{18dhr\mu^2\left(d+\psi\coth\left(\frac{1}{2}\psi\varpi\right)\right)}{w} \end{array} \right),$$

$$E_{4,4}(y,z,t) = \frac{\sigma}{\mu} \left(\begin{array}{c} \dfrac{v-d^2h\mu^2\sigma-8hrx\mu^2\sigma}{(q+r)\sigma} + \dfrac{16hw^2x^2\mu^2}{3(q+r)\left(d+\psi\coth\left(\frac{1}{2}\psi\varpi\right)\right)^2} + \dfrac{8dhwx\mu^2}{(q+r)\left(d+\psi\coth\left(\frac{1}{2}\psi\varpi\right)\right)} \\[3mm] +\dfrac{6dhr\mu^2\left(d+\psi\coth\left(\frac{1}{2}\psi\varpi\right)\right)}{(q+r)w} - \dfrac{3hr^2\mu^2\left(d+\psi\coth\left(\frac{1}{2}\psi\varpi\right)\right)^2}{(q+r)w^2} \end{array} \right).$$

5. Results and Discussion

The nonlinear coupled RW equations were solved analytically using three distinct types of derivative operator in this paper: conformable, beta, and M-truncated. These solutions were obtained using the efficient techniques named JEFM and MAEM. The methods produced several solutions, and the resulting solutions for three distinct derivative operators are contrasted in 2D graphs. The aforementioned techniques are used to produce solitary waves in a variety of shapes, including bell and smooth bell solitons, anti-bell solitons, periodic shape solitons, single kink solitons, and M- and W-shaped soliton solutions. Two-dimensional line graphs provide a very helpful comparison of the different fractional derivatives, such as β, conformable, and M-Truncated derivatives. It can be observed that the solitary waves slightly change when the parameter's value is varied without changing their curve form, which shows that their travelling wave solutions are symmetrical. The soliton solutions were obtained using the JEFM and MAEM. Using Wolfram Mathematica 10, these travelling wave solutions were verified. Figures 1–11 were produced by the same computer programme. They visually demonstrate how solitary waves behave in terms of both space and time. We looked at the composition of the solution. The graphs in the analytical solution clearly demonstrate that the JEFM and MAEM are more trustworthy and efficient. We discovered a range of solutions with various parameters when we solved the nonlinear coupled RW equation. These unnamed aspects affect the findings' character; if the parameters take on different specific values, several kinds of

solutions can be produced from a single solution. The following shows the impact of the solution-related factors. Regarding the 2D and 3D graphs of $R_{1,1}(y, 1, t)$, $R_{2,1}(y, 1, t)$, $R_{3,1}(y, 1, t)$, $E_{1,1}(y, 1, t)$, $E_{2,1}(y, 1, t)$, and $E_{3,1}(y, 1, t)$, respectively, we obtained the periodic wave solutions by considering the values m $= 0.5$, r $= 1.5, -1.5$, q $= 0.9$, $\sigma = 0.1$, h $= 2, -5$, $\mu = 0.9$, and v $= 0.7$ within the range $0 \leq y \leq 10, 0 \leq t \leq 6$ for 3D graphs and t = 1 for 2D plots, as shown in Figures 1–3 by JEFM. Figures 4 and 5 represent the bell-shaped and bright soliton 3D solutions of $R_{1,1}(y, 1, t)$, $R_{1,3}(y, 1, t)$, $E_{1,1}(y, 1, t)$, and $E_{1,3}(y, 1, t)$, and 2D plots for the unknown constants at t= 1, h $= 2.5$, x $= 0.1$, d $= 1.5$, w $= 1.7$, r $= 1.7$, $\sigma = 0.5$, $\mu = 0.7$, v= $0.1, 0.5$, q $= 1$, within the interval $-10 \leq y \leq 10, 0 \leq t \leq 5$ by MAEM. The hyperbolic and trigonometric function solutions in $R_{2,1}(y, 1, t)$, $R_{2,3}(y, 1, t)$, $E_{2,1}(y, 1, t)$ and $E_{2,3}(y, 1, t)$ were used to receive the corresponding anti-bell solitons and dark solitary solutions by taking the values h $= -2.5, -2.8$, x $= 0.1$, d $= 1.5$, w $= 1.7$, r $= 1.7$, $\sigma = 0.5$, $\mu = 0.7$, v= 0.1, q $= 1$, within the range $-10 \leq y \leq 10, 0 \leq t \leq 5$, and t = 1 for 2D plots in Figures 6 and 7. For the trigonometric solution in $R_{3,1}(y, 1, t)$, $R_{3,3}(y, 1, t)$, $E_{3,1}(y, 1, t)$ and $E_{3,3}(y, 1, t)$, we received the corresponding M-shape and W-shape solitary solutions by choosing the values h $= -2.5$, x $= 0.01$, d $= 1.5$, w $= 1.7$, r $= 1.7$, $\sigma = 0.5$, $\mu = 0.9$, v= 0.1, q $= 1$, within the range $-10 \leq y \leq 10, 0 \leq t \leq 5$, and t = 1 for 2D plots in Figures 8 and 9. The hyperbolic function solution in $R_{4,1}(y, 1, t)$, $R_{4,3}(y, 1, t)$, $E_{4,1}(y, 1, t)$ and $E_{4,3}(y, 1, t)$, serving as the kink-type wave soliton and single-wave solutions, respectively, can be obtained by taking the values h $= 2.5$, x $= 0.1$, d $= 1.5$, w $= 1.7$, r $= 1.7$, $\sigma = 0.5$, $\mu = 0.5$, v $= 0.1$, q $= 1$, within the range $-10 \leq y \leq 10, 0 \leq t \leq 6$, and t = 1 for 2D plots in Figures 10 and 11. Figures 1–11 show that each pair of travelling solutions have a symmetrical mathematical form.

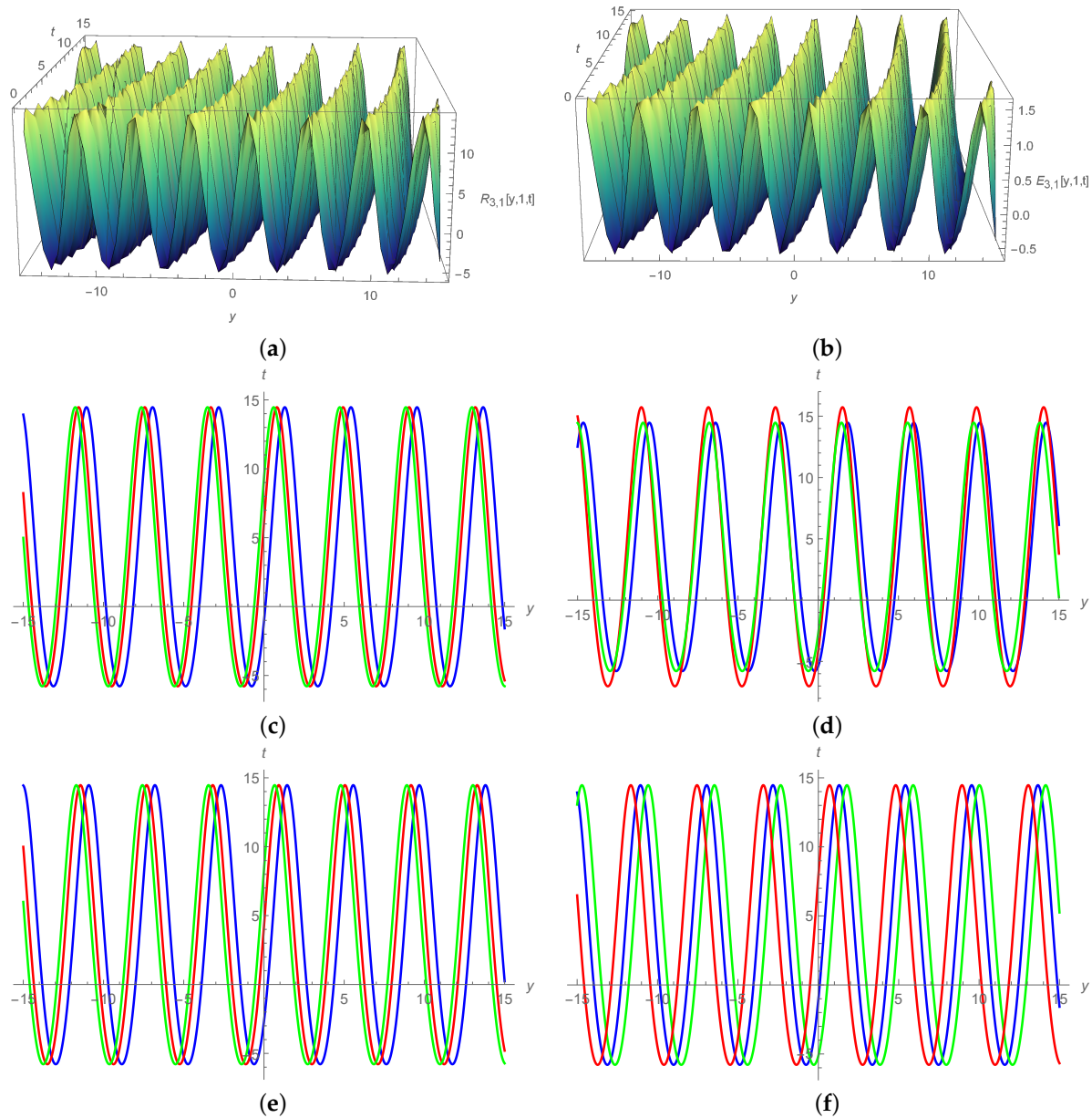(**a**)
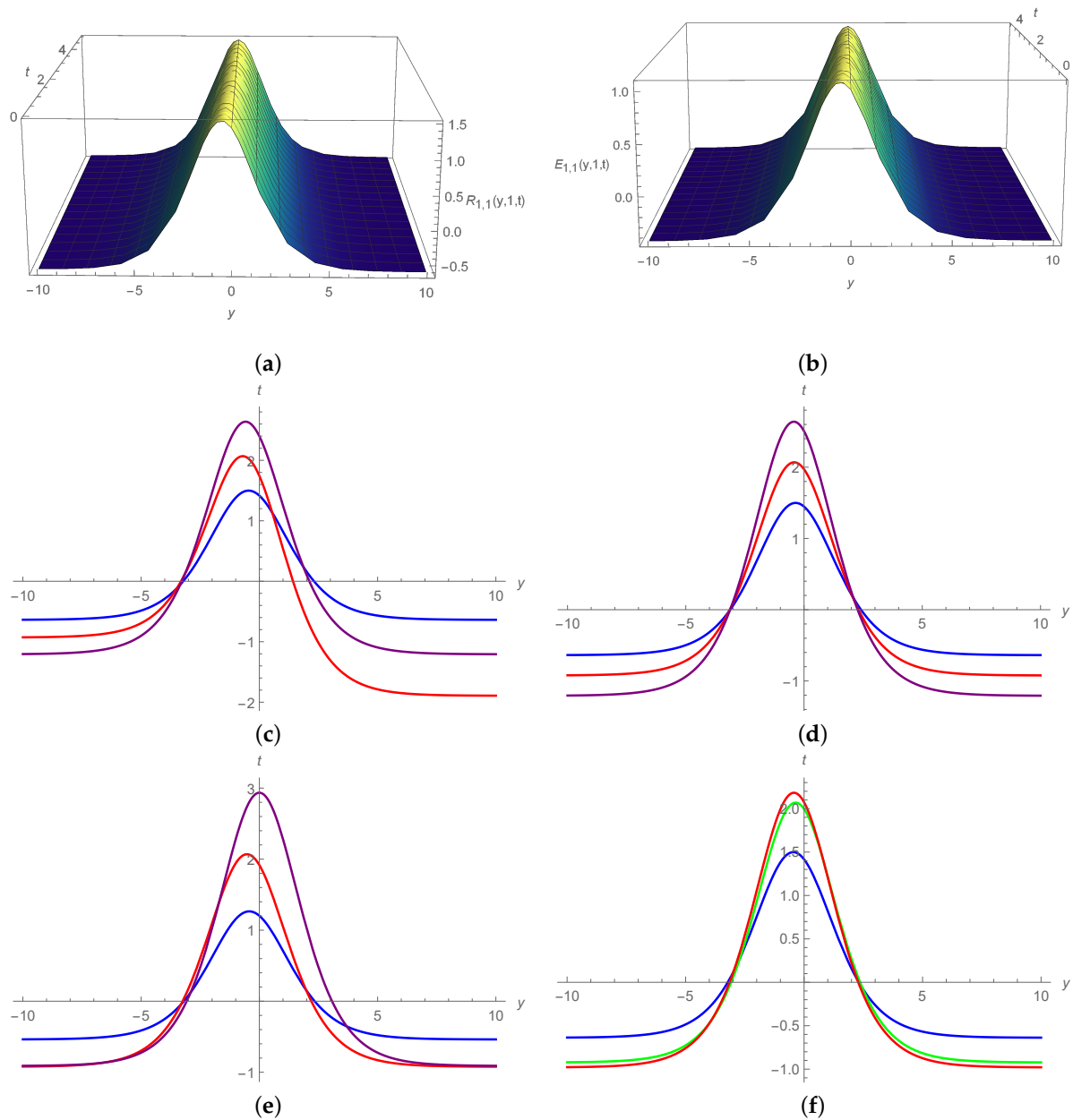

(**b**)


(**c**)

(**d**)

(**e**)

(**f**)
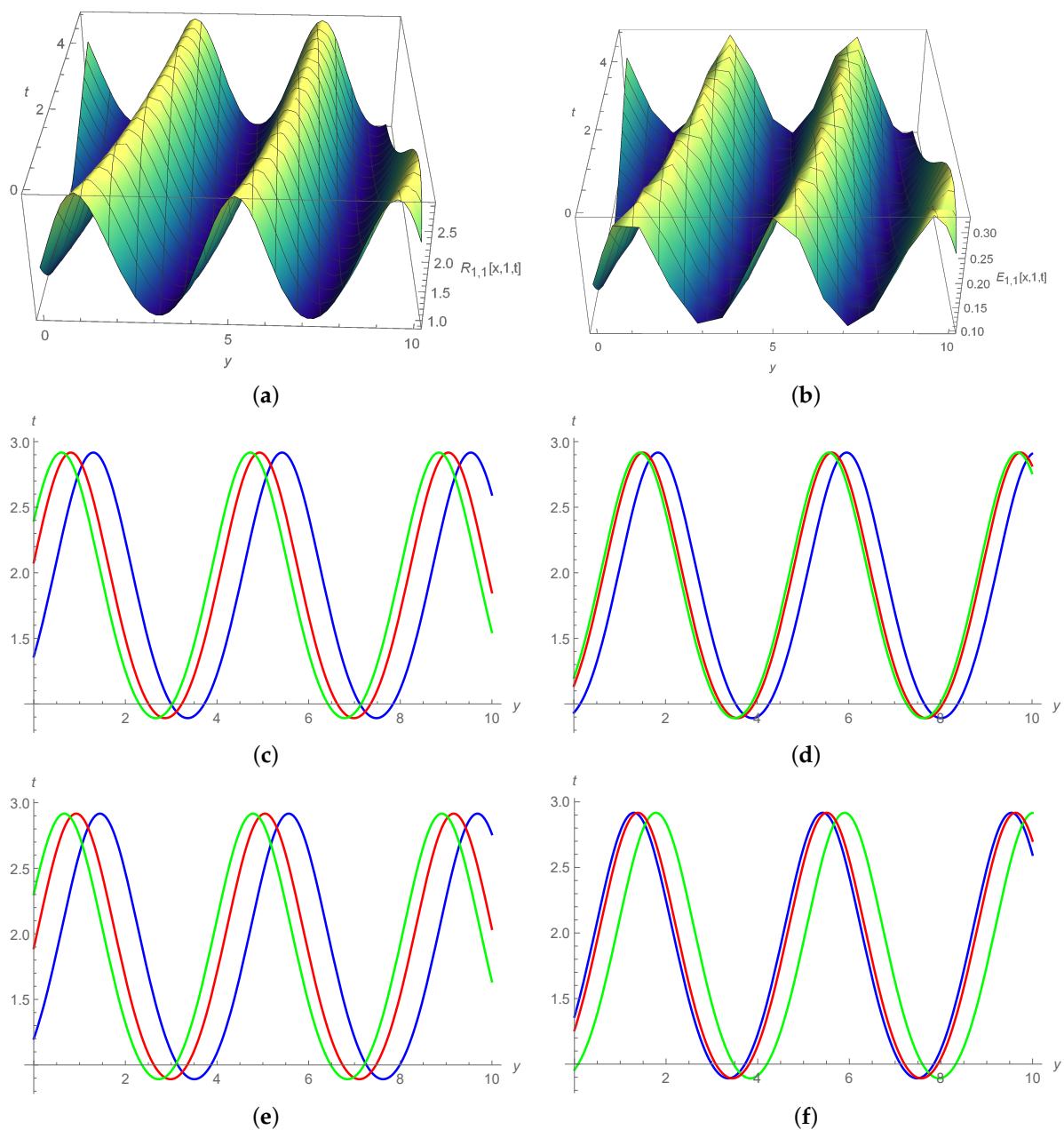
Figure 1. Graphical presentation of the analytical solutions by JEFM: when $m = 0.5, r = 1.5, q = 0.9,$ $\sigma = 0.1, h = 2, \mu = 0.9, v = 0.7$. (**c–e**): corresponding 2D plots at $t = 1$. (**a**) β-D 3D graph at $\delta = 0.5$ for $R_{1,1}(y, 1, t)$. (**b**) β-D 3D graph at $\delta = 0.5$ for $E_{1,1}(y, 1, t)$. (**c**) 2D plot of M-TD at different values of $\delta = 0.5, \chi = 0.25$ (blue), $\delta = 0.75, \chi = 0.5$ (red) ,$\delta = 1, \chi = 0.75$ (green) for $R_{1,1}(y, 1, 1)$. (**d**) 2D plot of β-D at different values of $\delta = 0.5$ (blue),0.75 (red), 1 (green) for $R_{1,1}(y, 1, 1)$. (**e**) 2D plot of C-D at different values of $\delta = 0.5$ (blue), 0.75 (red), 1 (green) for $R_{1,1}(y, 1, 1)$. (**f**) A comparison between M-TD (blue), β-D (green) and C-D (red) at $\delta = 0.5$ for $R_{1,1}(y, 1, 1)$.
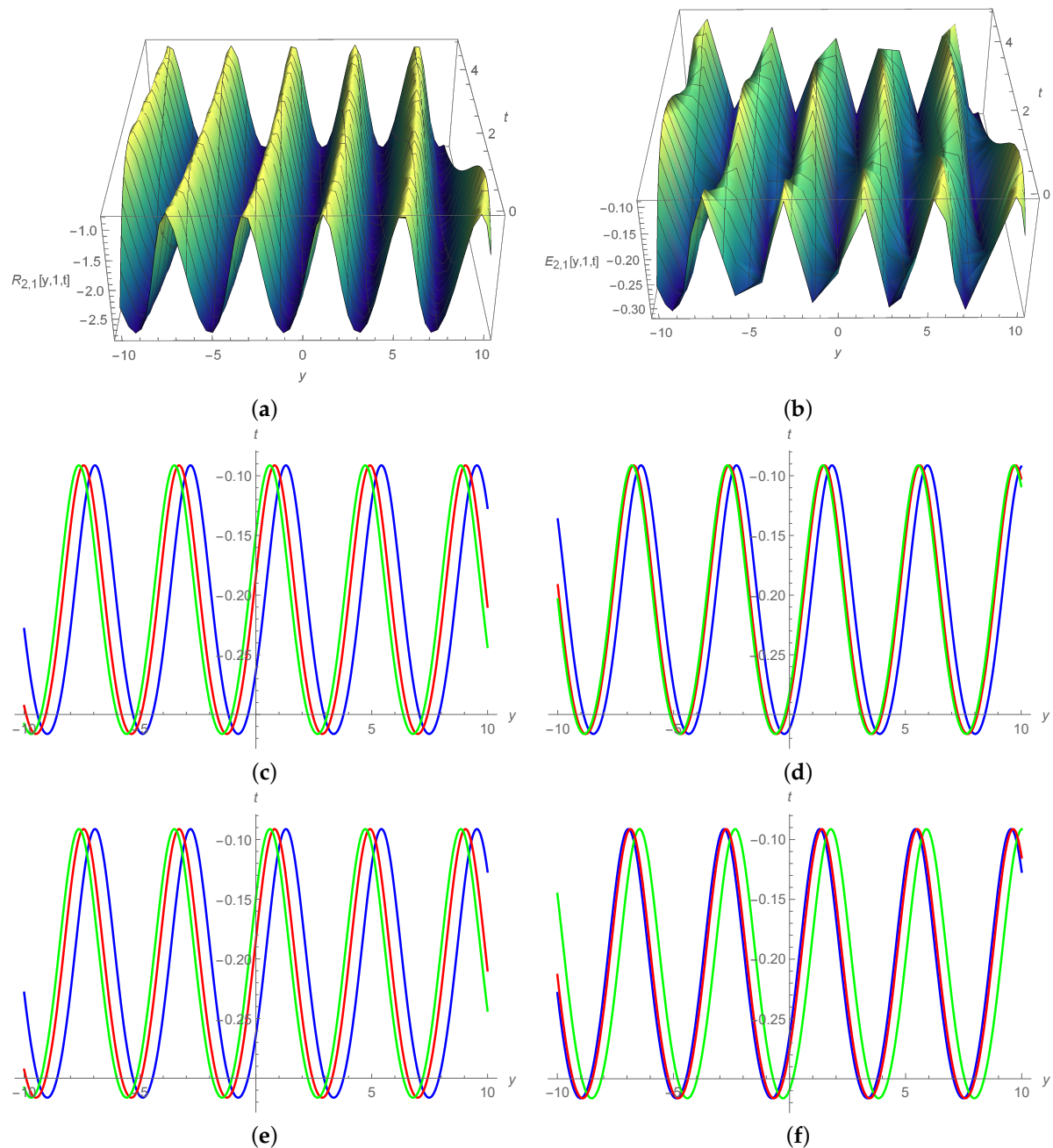
Figure 2. Graphical presentation of the analytical solutions by JEFM: when $m = 0.5, r = 1.5, q = 0.9,$ $\sigma = 0.1, h = 2, \mu = 0.9, v = 0.7$. (**c**–**e**): corresponding 2D plots at $t = 1$. (**a**) β-D 3D graph at $\delta = 0.5$ for $R_{2,1}(y, 1, t)$. (**b**) β-D 3D graph at $\delta = 0.5$ for $E_{2,1}(y, 1, t)$. (**c**) 2D plot of M-TD at different values of $\delta = 0.5, \chi = 0.25$ (blue), $\delta = 0.75, \chi = 0.5$ (red) ,δ=1,χ = 0.75(green) for $E_{2,1}(y, 1, 1)$. (**d**) 2D plot of β-D at different values of $\delta = 0.5$ (blue), 0.75 (red), 1 (green) for $E_{2,1}(y, 1, 1)$. (**e**) 2D plot of C-D at different values of $\delta = 0.5$ (blue), 0.75 (red), 1 (green) for $E_{2,1}(y, 1, 1)$. (**f**) A comparison between M-TD (blue), β-D (green) and C-D (red) at $\delta = 0.5$ for $E_{2,1}(y, 1, 1)$.

(a)

(b)

(c)

(d)

(e)

(f)

Figure 3. Graphical presentation of the analytical solutions by JEFM: when $m = 0.5, r = -1.5, q = 0.9,$ $\sigma = 0.1, h = -5, \mu = 0.9, v = 0.7$. (**c–e**): corresponding 2D plots at $t = 1$. (**a**) β-D 3D graph at $\delta = 0.5$ for $R_{3,1}(y, 1, t)$. (**b**) β-D 3D graph at $\delta = 0.5$ for $E_{3,1}(y, 1, t)$. (**c**) 2D plot of M-TD at different values of $\delta = 0.5, \chi = 0.25$ (blue), $\delta = 0.75, \chi = 0.5$ (red), $\delta = 1, \chi = 0.75$ (green) for $R_{3,1}(y, 1, 1)$. (**d**) 2D plot of β-D at different values of $\delta = 0.5$ (blue), 0.75 (red), 1 (green) for $R_{3,1}(y, 1, 1)$. (**e**) 2D plot of C-D at different values of $\delta = 0.5$ (blue), 0.75 (red), 1 (green) for $R_{3,1}(y, 1, 1)$. (**f**) A comparison between M-TD (blue), β-D (green) and C-D (red) at $\delta = 0.5$ for $R_{3,1}(y, 1, 1)$.
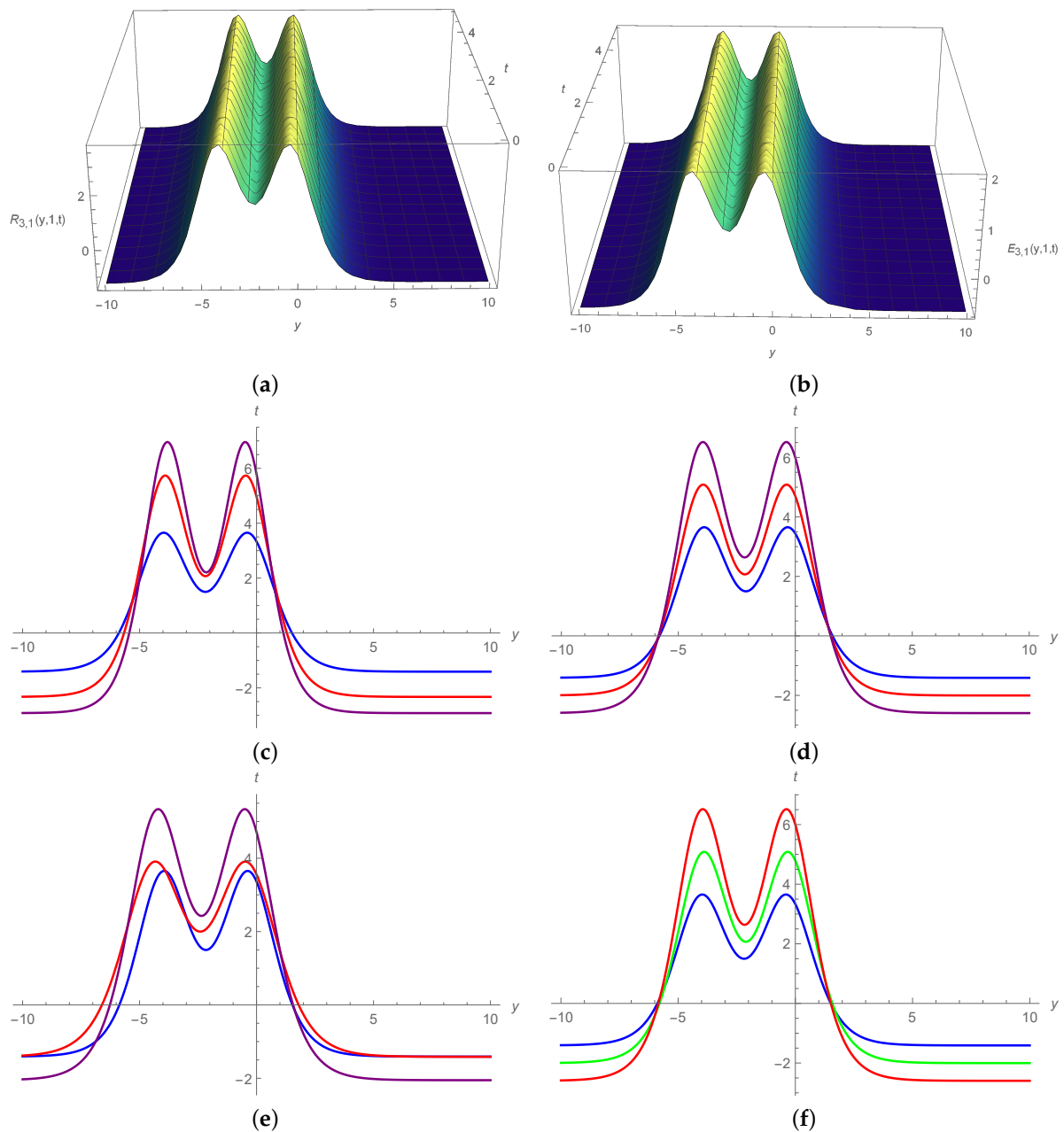
Figure 4. Graphical presentation of the analytical solutions by MAEM: when $h = 2.5, x = 0.1$, $d = 1.5, w = 1.7, r = 1.7, \sigma = 0.5, \mu = 0.7, v = 0.1, q = 1$. (**c**–**e**): corresponding 2D plots at $t = 1$. (**a**) β-D 3D graph at $\delta = 0.5$ for $R_{1,1}(y, 1, t)$. (**b**) β-D 3D graph at $\delta = 0.5$ for $E_{1,1}(y, 1, t)$. (**c**) 2D plot of M-TD at different values of $\delta = 0.5$, $\chi = 0.25$ (blue), $\delta = 0.75$, $\chi = 0.5$ (red), $\delta = 1$, $\chi = 0.75$ (purple) for $R_{1,1}(y, 1, 1)$. (**d**) 2D plot of β-D at different values of $\delta = 0.5$ (blue), 0.75 (red), 1 (purple) for $R_{1,1}(y, 1, 1)$. (**e**) 2D plot of C-D at different values of $\delta = 0.5$ (blue), 0.75 (red), 1 (purple) for $R_{1,1}(y, 1, 1)$. (**f**) A comparison between M-TD (blue), β-D (green) and C-D (red) at $\delta = 0.5$ for $R_{1,1}(y, 1, 1)$.

(a)

(b)

(c)

(d)

(e)

(f)
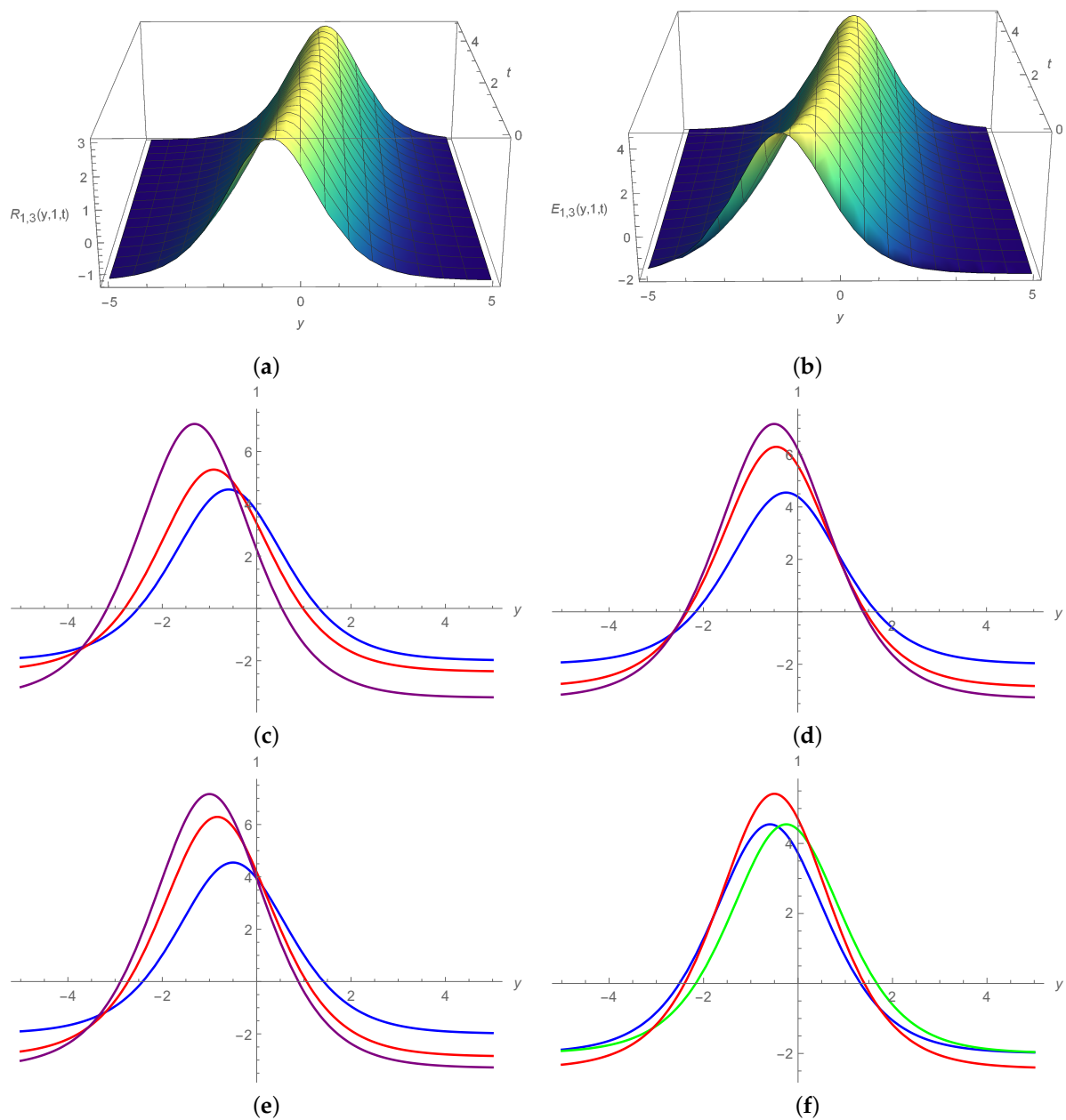
Figure 5. Graphical presentation of the analytical solutions by MAEM: when $h = 2.5, x = 0.1,$ $d = 1.5, w = 1.7, r = 1.7, \sigma = 1.5, \mu = 1, v = 0.5, q = 1.$ (**c**–**e**): corresponding 2D plots at $t = 1$. (**a**) β-D 3D graph at $\delta = 0.5$ for $R_{1,3}(y, 1, t)$. (**b**) β-D 3D graph at $\delta = 0.5$ for $E_{1,3}(y, 1, t)$. (**c**) 2D plot of M-TD at different values of $\delta = 0.5$, $\chi = 0.25$ (blue), $\delta = 0.75$, $\chi = 0.5$ (red), $\delta = 1$, $\chi = 0.75$ (purple) for $E_{1,3}(y, 1, 1)$. (**d**) 2D plot of β-D at different values of $\delta = 0.5$ (blue), 0.75 (red), 1 (purple) for $E_{1,3}(y, 1, 1)$. (**e**) 2D plot of C-D at different values of $\delta = 0.5$ (blue), 0.75 (red), 1 (purple) for $E_{1,3}(y, 1, 1)$. (**f**) A comparison between M-TD (blue), β-D (green) and C-D (red) at $\delta = 0.5$ for $E_{1,3}(y, 1, 1)$.
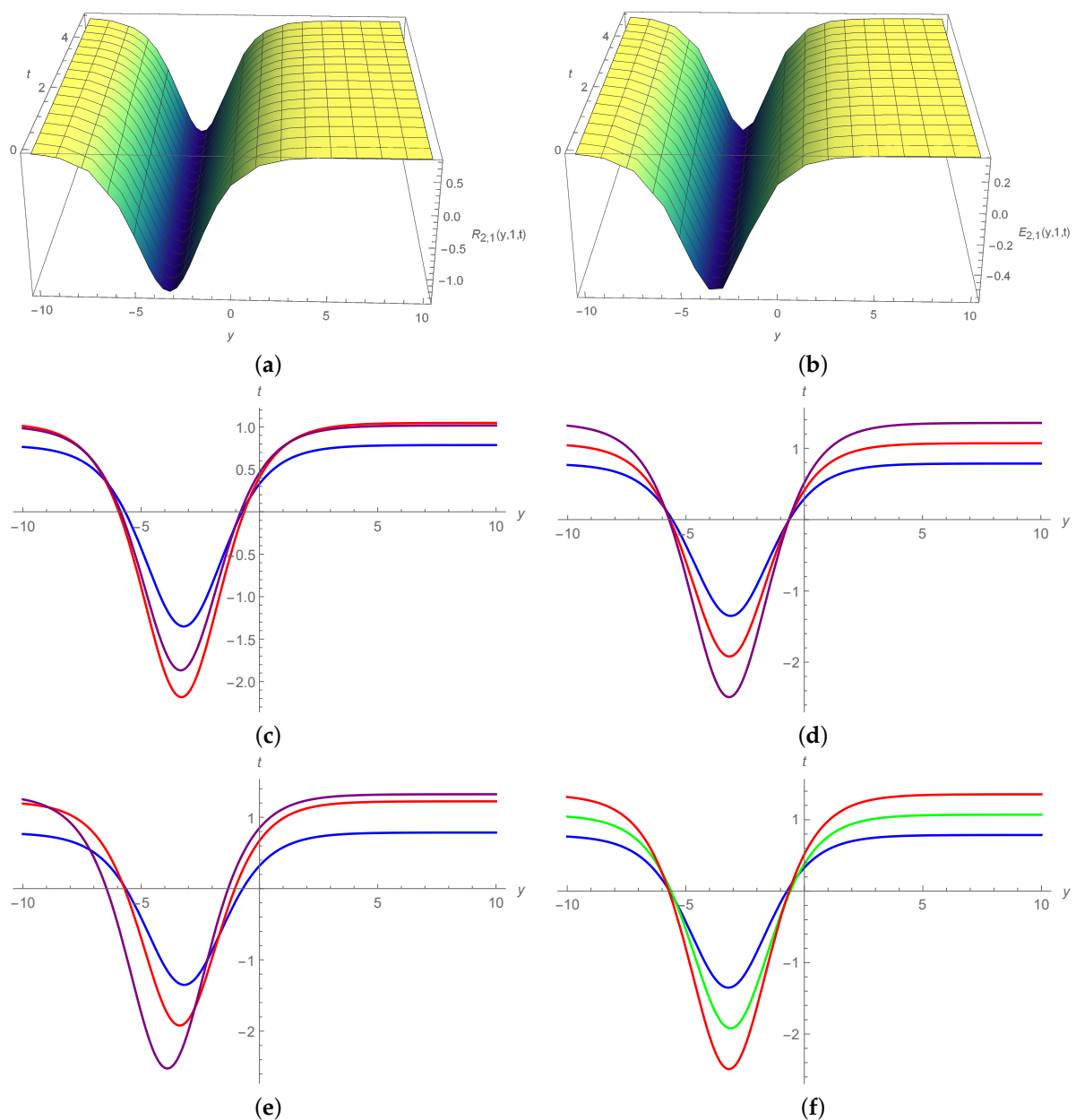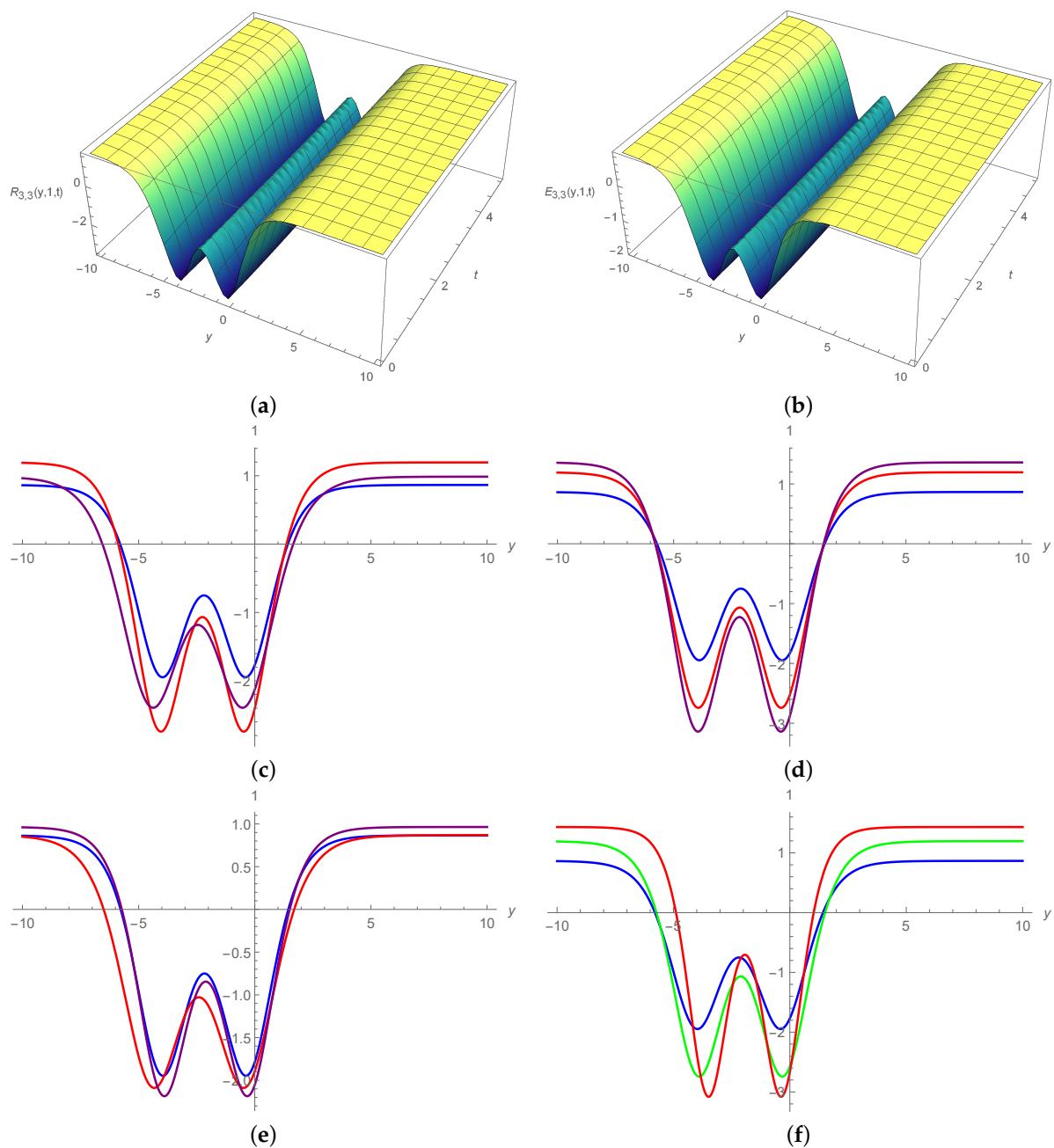
Figure 6. Graphical presentation of the analytical solutions by MAEM: when $h = -2.5, x = 0.1$, $d = 1.5, w = 1.7, r = 1.7, \sigma = 0.5, \mu = 0.7, v = 0.1, q = 1$. (**c**–**e**):corresponding 2D plots at $t = 1$. (**a**) β-D 3D graph at $\delta = 0.5$ for $R_{2,1}(y, 1, t)$. (**b**) β-D 3D graph at $\delta = 0.5$ for $E_{2,1}(y, 1, t)$. (**c**) 2D plot of M-TD at different values of $\delta = 0.5$, $\chi = 0.25$ (blue), $\delta = 0.75$, $\chi = 0.5$ (red), $\delta = 1$, $\chi = 0.75$ (purple) for $R_{2,1}(y, 1, 1)$. (**d**) 2D plot of β-D at different values of $\delta = 0.5$ (blue), 0.75 (red), 1 (purple) for $R_{2,1}(y, 1, 1)$. (**e**) 2D plot of C-D at different values of $\delta = 0.5$ (blue), 0.75 (red), 1 (purple) for $R_{2,1}(y, 1, 1)$. (**f**) A comparison between M-TD (blue), β-D (green) and C-D (red) at $\delta = 0.5$ for $R_{2,1}(y, 1, 1)$.
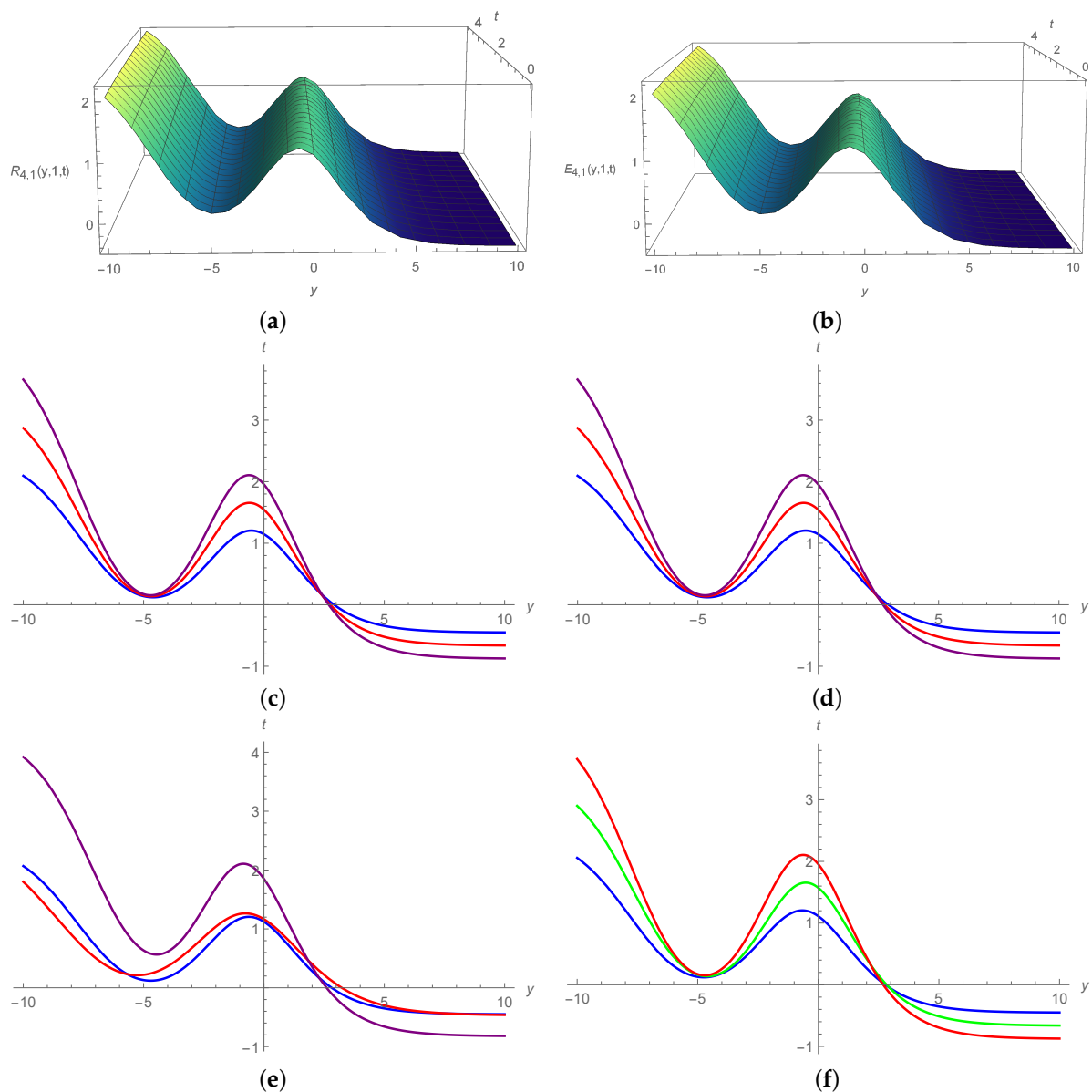
(a)

(b)

(c)

(d)

(e)

(f)
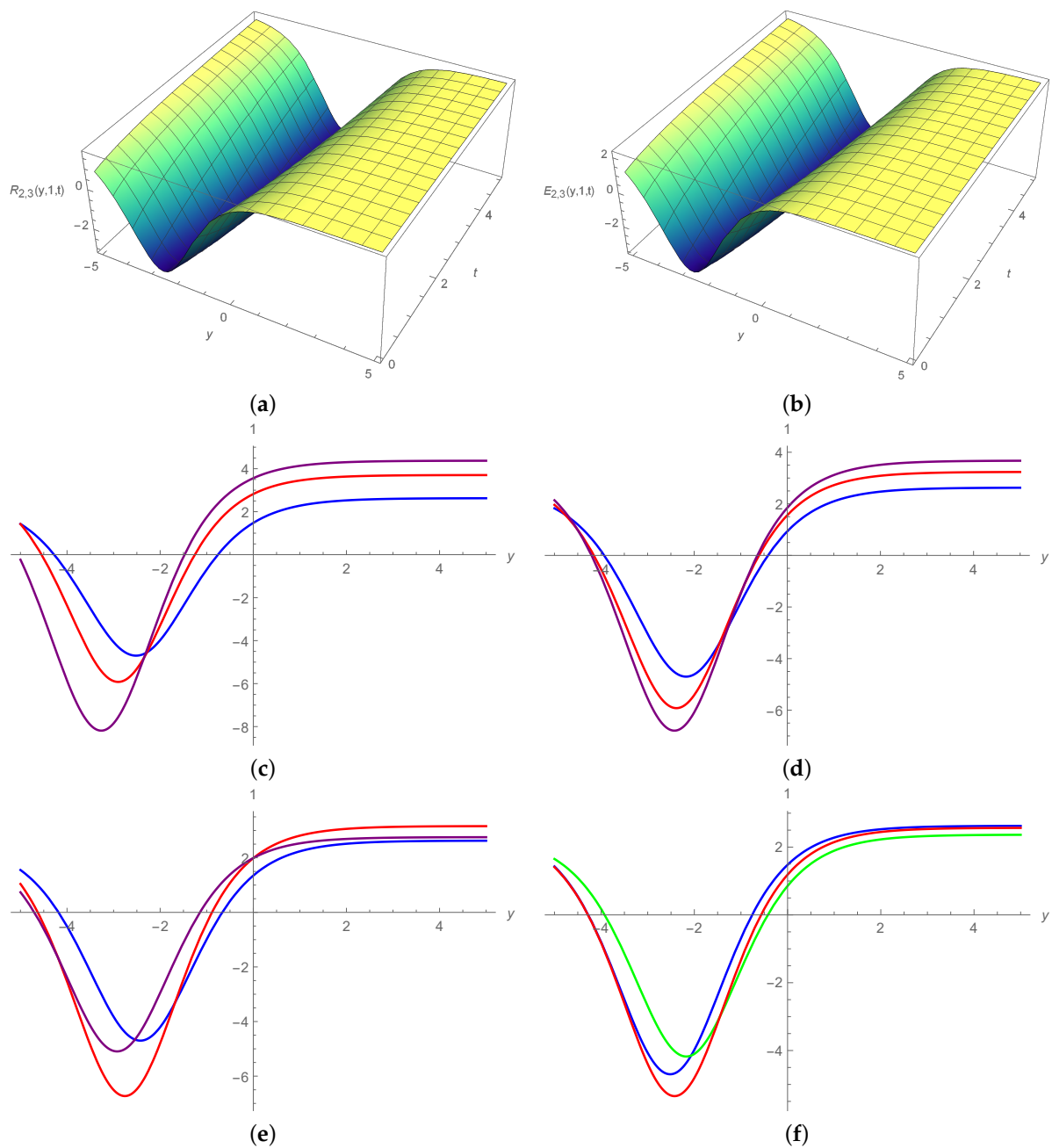
Figure 7. Graphical presentation of the analytical solutions by MAEM: when $h = -2.8, x = 0.1$, $d = 1.5, w = 1.7, r = 1.7, \sigma = 1.5, \mu = 1, v = 0.5, q = 1$. (**c**–**e**): corresponding 2D plots at $t = 1$. (**a**) β-D 3D graph at $\delta = 0.5$ for $R_{2,3}(y, 1, t)$. (**b**) β-D 3D graph at $\delta = 0.5$ for $E_{2,3}(y, 1, t)$. (**c**) 2D plot of M-TD at different values of $\delta = 0.5, \chi = 0.25$ (blue), $\delta = 0.75$, $\chi = 0.5$ (red) ,$\delta=1$, $\chi = 0.75$ (purple) for $E_{2,3}(y, 1, 1)$. (**d**) 2D plot of β-D at different values of $\delta = 0.5$ (blue), 0.75 (red), 1 (purple) for $E_{2,3}(y, 1, 1)$. (**e**) 2D plot of C-D at different values of $\delta = 0.5$ (blue), 0.75 (red), 1 (purple) for $E_{2,3}(y, 1, 1)$. (**f**) A comparison between M-TD (blue), β-D (green) and C-D (red) at $\delta = 0.5$ for $E_{2,3}(y, 1, 1)$.

Figure 8. Graphical presentation of the analytical solutions by MAEM: when $h = 2.5, x = 0.01$, $d = 1.5, w = 1.7, r = 1.7, \sigma = 0.5, \mu = 0.9, v = 0.1, q = 1$. (**c–e**):corresponding 2D plots at $t = 1$. (**a**) β-D 3D graph at $\delta = 0.5$ for $R_{3,1}(y, 1, t)$. (**b**) β-D 3D graph at $\delta = 0.5$ for $E_{3,1}(y, 1, t)$. (**c**) 2D plot of M-TD at different values of $\delta = 0.5$, $\chi = 0.25$ (blue), $\delta = 0.75$, $\chi = 0.5$ (red), $\delta = 1$, $\chi = 0.75$ (purple) for $R_{3,1}(y, 1, 1)$. (**d**) 2D plot of β-D at different values of $\delta = 0.5$ (blue), 0.75 (red), 1 (purple) for $R_{3,1}(y, 1, 1)$. (**e**) 2D plot of C-D at different values of $\delta = 0.5$ (blue), 0.75 (red), 1 (purple) for $R_{3,1}(y, 1, 1)$. (**f**) A comparison between M-TD (blue), β-D (green) and C-D (red) at $\delta = 0.5$ for $R_{3,1}(y, 1, 1)$.

Figure 9. Graphical presentation of the analytical solutions by MAEM: when $h = -2.5$, $x = 0.01$, $d = 1.5$, $w = 1.7$, $r = 1.7$, $\sigma = 0.5$, $\mu = 0.9$, $v = 0.1$, $q = 1$. (**c**–**e**): corresponding 2D plots at $t = 1$. (**a**) β-D 3D graph at $\delta = 0.5$ for $R_{3,3}(y, 1, t)$. (**b**) β-D 3D graph at $\delta = 0.5$ for $E_{3,3}(y, 1, t)$. (**c**) 2D plot of M-TD at different values of $\delta = 0.5$, $\chi = 0.25$ (blue), $\delta = 0.75$, $\chi = 0.5$ (red), $\delta = 1$, $\chi = 0.75$ (purple) for $E_{3,3}(y, 1, 1)$. (**d**) 2D plot of β-D at different values of $\delta = 0.5$ (blue), 0.75 (red), 1 (purple) for $E_{3,3}(y, 1, 1)$. (**e**) 2D plot of C-D at different values of $\delta = 0.5$ (blue), 0.75 (red), 1 (purple) for $E_{3,3}(y, 1, 1)$. (**f**) A comparison between M-TD (blue), β-D (green) and C-D (red) at $\delta = 0.5$ for $E_{3,3}(y, 1, 1)$.

Figure 10. Graphical presentation of the analytical solutions by MAEM: when $h = 2.5, x = 0.01$, $d = 1.5, w = 1.5, r = 1.5, \sigma = 0.5, \mu = 0.5, v = 0.1, q = 1$. (**c–e**): corresponding 2D plots at $t = 1$. (**a**) β-D 3D graph at $\delta = 0.5$ for $R_{4,1}(y, 1, t)$. (**b**) β-D 3D graph at $\delta = 0.5$ for $E_{4,1}(y, 1, t)$. (**c**) 2D plot of M-TD at different values of $\delta = 0.5$, $\chi = 0.25$ (blue), $\delta = 0.75$, $\chi = 0.5$ (red), $\delta = 1$, $\chi = 0.75$ (purple) for $R_{4,1}(y, 1, 1)$. (**d**) 2D plot of β-D at different values of $\delta = 0.5$ (blue), 0.75 (red), 1 (purple) for $R_{4,1}(y, 1, 1)$. (**e**) 2D plot of C-D at different values of $\delta = 0.5$ (blue), 0.75 (red), 1 (purple) for $R_{4,1}(y, 1, 1)$. (**f**) A comparison between M-TD (blue), β-D (green) and C-D (red) at $\delta = 0.5$ for $R_{4,1}(y, 1, 1)$.

(a)

(b)

(c)

(d)

(e)

(f)
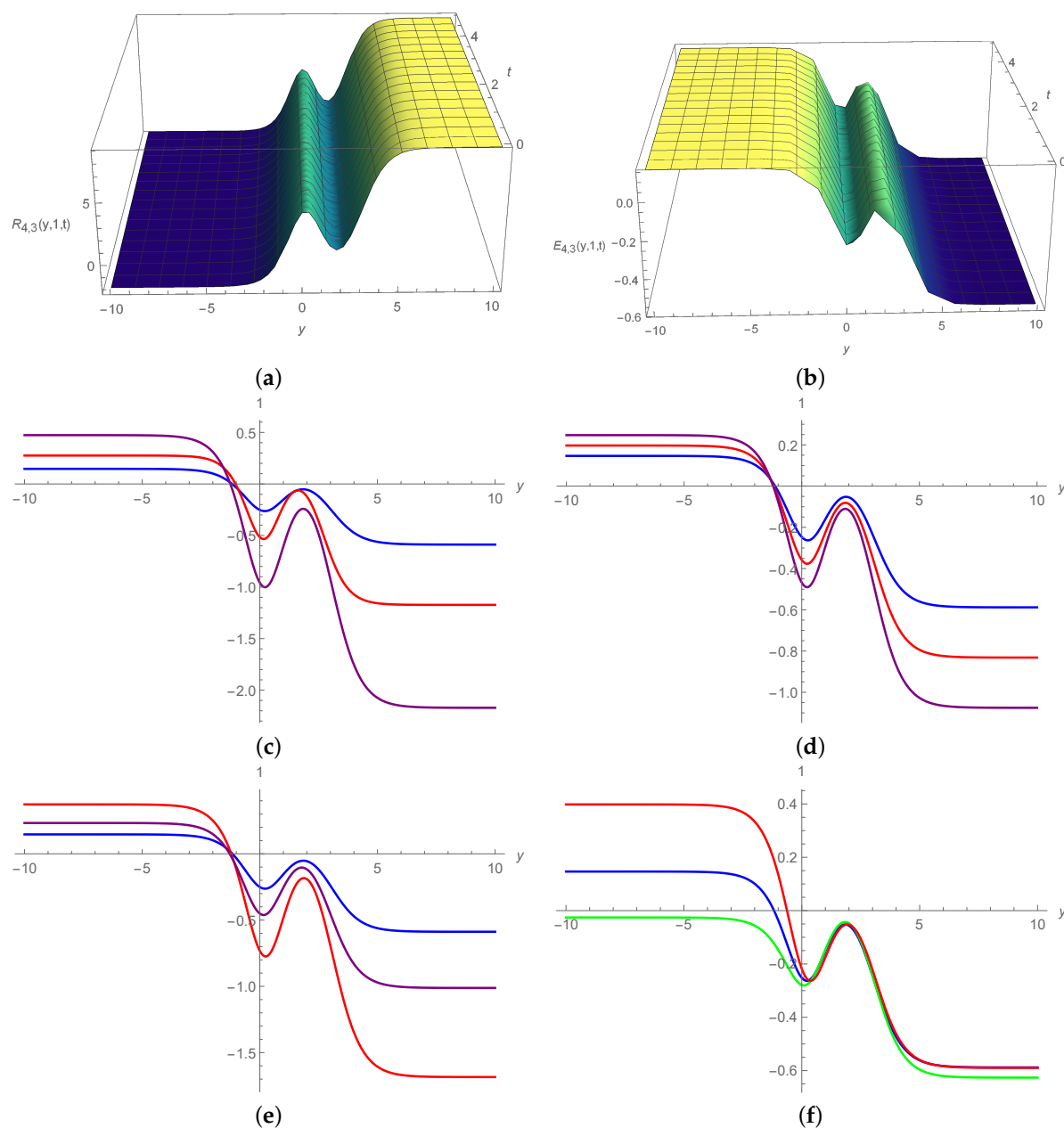
Figure 11. Analytical solutions by MAEM: when $h = 2.5, x = 0.01, d = 1.1, w = 1.7, r = 1.7, \sigma = 0.1$, $\mu = -1.5, v = -0.1, q = 1.5$. (**c**–**e**): corresponding 2D plots at $t = 1$. (**a**) β-D 3D graph at $\delta = 0.5$ for $R_{4,3}(y, 1, t)$. (**b**) β-D 3D graph at $\delta = 0.5$ for $E_{4,3}(y, 1, t)$. (**c**) 2D plot of M-TD at different values of $\delta = 0.5, \chi = 0.25$ (blue), $\delta = 0.75, \chi = 0.5$ (red), $\delta = 1, \chi = 0.75$ (purple) for $E_{4,3}(y, 1, 1)$. (**d**) 2D plot of β-D at different values of $\delta = 0.5$ (blue), 0.75 (red), 1 (purple) for $E_{4,3}(y, 1, 1)$. (**e**) 2D plot of C-D at different values of $\delta = 0.5$ (blue), 0.75 (red), 1 (purple) for $E_{4,3}(y, 1, 1)$. (**f**) A comparison between M-TD(blue), β-D (green) and C-D (red) at $\delta = 0.5$ for $E_{4,3}(y, 1, 1)$.

6. Conclusions

In this paper, analytical solutions to the nonlinear coupled Riemann wave (RW) equations were found using the modified auxiliary equation and Jacobi elliptic function techniques. We developed solitary wave solutions for each of the examined equations that contain certain unknown parameters. The periodic wave solution, bright, dark, or anti-bell-shaped soliton solutions, M-shaped, W-shaped soliton solutions, and kink-type soliton solutions were obtained using the concepts of fractional derivatives, i.e., β, conformable, and M-truncated derivatives. This paper analyses the derivatives on a comparative basis.

According to the results, all the derivatives are satisfactory, but β-D has a better form. The discovered solutions will help in the study of problems related to engineering, mechanical theory, tsunamis, and tidal waves. The fractional derivative's impact on the analytical solution of the RW equation was finally illustrated using the Mathematica tools in Figures 1–11.

References

1. Ablowitz, M.J.; Ramani, A.; Segur, H. Nonlinear evolution equations and ordinary differential equations of Painleve'type. *Lett. Nuovo Cim.* **1978**, *23*, 333–338. [CrossRef]
2. Tikhonov, A.N.; Samarskiy, A.A. *Equations of Mathematical Physics*; Moscow University Press: Moscow, Russia, 1999.
3. Renardy, M.; Rogers, R.C. *An Introduction to Partial Differential Equations*; Springer Science & Business Media: Berlin/Heidelberg, Germany, 2006.
4. Suret, P.; Tikan, A.; Bonnefoy, F.; Copie, F.; Ducrozet, G.; Gelash, A.; Prabhudesai, G.; Michel, G.; Cazaubiel, A.; Falcon, E.; et al. Nonlinear spectral synthesis of soliton gas in deep-water surface gravity waves. *Phys. Rev. Lett.* **2020**, *125*, 264101. [CrossRef]
5. Barkan, A.; D'angelo, N.; Merlino, R.L. Experiments on ion-acoustic waves in dusty plasmas. *Planet. Space Sci.* **1996**, *44*, 239–242. [CrossRef]
6. Dalir, M.; Bashour, M. Applications of fractional calculus. *Appl. Math. Sci.* **2010**, *4*, 1021–1032.
7. Kilbas, A.A.; Srivastava, H.M.; Trujillo, J.J. *Theory and Applications of Fractional Differential Equations*; Elsevier: Amsterdam, The Netherlands, 2006
8. Sun, H.; Zhang, Y.; Baleanu, D.; Chen, W.; Chen, Y. A new collection of real world applications of fractional calculus in science and engineering. *Commun. Nonlinear Sci. Numer. Simul.* **2018**, *64*, 213–231. [CrossRef]
9. Arnol'd, V.I. *Geometrical Methods in the Theory of Ordinary Differential Equations*; Springer: Heidelberg/Berlin, Germany, 1983.
10. Almeida, R. A Caputo fractional derivative of a function with respect to another function. *Commun. Nonlinear Sci. Numer. Simul.* **2017**, *44*, 460–481. [CrossRef]
11. Garg, V.; Singh, K. An improved Grunwald-Letnikov fractional differential mask for image texture enhancement. *Int. J. Adv. Comput. Sci. Appl.* **2012**, *3*, 130–135. [CrossRef]
12. Onder, I.; Cinar, M.; Secer, A.; Bayram, M. Analytical solutions of simplified modified Camassa-Holm equation with conformable and M-truncated derivatives: A comparative study. *J. Ocean. Eng. Sci.* **2022**, *in press*. [CrossRef]
13. Atangana, A.; Koca, I. Chaos in a simple nonlinear system with Atangana–Baleanu derivatives with fractional order. *Chaos Solitons Fractals* **2016**, *89*, 447–454. [CrossRef]
14. Atangana, A.; Doungmo Goufo, E.F. Extension of matched asymptotic method to fractional boundary layers problems. *Math. Probl. Eng.* **2014**, *2014*, 107535. [CrossRef]
15. Hussain, A.; Jhangeer, A.; Abbas, N.; Khan, I.; Sherif, E.S.M. Optical solitons of fractional complex Ginzburg–Landau equation with conformable, beta, and M-truncated derivatives: A comparative study. *Adv. Differ. Eq.* **2020**, *2020*, 1–19. [CrossRef]
16. Alharbi, F.M.; Baleanu, D.; Ebaid, A. Physical properties of the projectile motion using the conformable derivative. *Chin. J. Phys.* **2019**, *58*, 18–28. [CrossRef]
17. Majid, S.Z.; Faridi, W.A.; Asjad, M.I.; Abd El-Rahman, M.; Eldin, S.M. Explicit Soliton Structure Formation for the Riemann Wave Equation and a Sensitive Demonstration. *Fractal Fract.* **2023**, *7*, 102. [CrossRef]
18. Barman, H.K.; Seadawy, A.R.; Akbar, M.A.; Baleanu, D. Competent closed form soliton solutions to the Riemann wave equation and the Novikov-Veselov equation. *Results Phys.* **2020**, *17*, 103131. [CrossRef]

19. Triggiani, R. Carleman estimates with no lower-order terms for general Riemann wave equations. Global uniqueness and observability in one shot. *Appl. Math. Optim.* **2002**, *46*, 331–375.

20. Shakeel, M.; Ahmad, B.; Shah, N.A.; Chung, J.D. Solitons Solution of Riemann Wave Equation via Modified Exp Function Method. *Symmetry* **2022**, *14*, 2574.

21. Parkes, E.J.; Duffy, B.R.; Abbott, P.C. The Jacobi elliptic-function method for finding periodic-wave solutions to nonlinear evolution equations. *Phys. Lett. A* **2002**, *295*, 280–286. [CrossRef]

22. Bashar, M.H.; Inc, M.; Islam, S.R.; Mahmoud, K.H.; Akbar, M.A. Soliton solutions and fractional effects to the time-fractional modified equal width equation. *Alex. Eng. J.* **2022**, *61*, 12539–12547. [CrossRef]

23. Podlubny, I. *Fractional Differential Equations: An Introduction to Fractional Derivatives, Fractional Differential Equations, to Methods of Their Solution and Some of Their Applications*; Academic Press: New York, NY, USA, 1998; p. 198.

24. Oldham, K.B.; Spanier, J. *The Fractional Calculus*; Academic Press: New York, NY, USA, 1974.

25. Singh, J.; Kumar, D.; Al Qurashi, M.; Baleanu, D. A new fractional model for giving up smoking dynamics. *Adv. Differ. Eq.* **2017**, *2017*, 88. [CrossRef]

26. Caputo, M.; Mainardi, F. A new dissipation model based on memory mechanism. *Pure Appl. Geophys.* **1971**, *91*, 134–147. [CrossRef]

27. Caputo, M.; Fabricio, M. A new definition of fractional derivative without singular kernel. *Prog. Fract. Differ. Appl.* **2019**, *1*, 73–85.

28. Atangana, A.; Baleanu, D. New fractional derivatives with nonlocal and non-singular kernel. Theory and application to heat transfer model. *Therm. Sci.* **2016**, *20*, 763–769. [CrossRef]

29. Khalil, R.; Al Horani, M.; Yousef, A.; Sababheh, M. A new definition of fractional derivative. *J. Comput. Appl. Math.* **2014**, *264*, 65–70. [CrossRef]

30. Atangana, A.; Baleanu, D.; Alsaedi, A. New properties of conformable derivative. *Open Math.* **2015**, *13*, 1–10. [CrossRef]

31. Hyder, A.A.; Soliman, A.H. An extended Kudryashov technique for solving stochastic nonlinear models with generalized conformable derivatives. *Commun. Nonlinear Sci. Numer. Simul.* **2021**, *97*, 105730. [CrossRef]

32. Arafat, S.Y.; Islam, S.R.; Rahman, M.M.; Saklayen, M.A. On nonlinear optical solitons of fractional Biswas-Arshed Model with beta derivative. *Results Phys.* **2023**, *48*, 106426. [CrossRef]

33. Atangana, A.; Baleanu, D.; Alsaedi, A. Analysis of time-fractional Hunter–Saxton equation: A model of neumatic liquid crystal. *Open Phys.* **2016**, *14*, 145–149. [CrossRef]

34. Pólya, G. On the mean-value theorem corresponding to a given linear homogeneous differential equation. *Trans. Am. Math. Soc.* **1922**, *24*, 312–324.

35. Kilbas, A.A.; Saigo, M.; Saxena, R.K. Generalized Mittag-Leffler function and generalized fractional calculus operators. *Integral Transform. Spec. Funct.* **2004**, *15*, 31–49. [CrossRef]

36. Serkin, V.N.; Hasegawa, A. Novel soliton solutions of the nonlinear Schrödinger equation model. *Phys. Rev. Lett.* **2000**, *85*, 4502. [CrossRef]

37. Fan, E.; Zhang, J. Applications of the Jacobi elliptic function method to special-type nonlinear equations. *Phys. Lett. A* **2002**, *305*, 383–392. [CrossRef]

38. Dai, C.; Zhang, J. Jacobian elliptic function method for nonlinear differential-difference equations. *Chaos Solitons Fractals* **2006**, *27*, 1042–1047. [CrossRef]

39. Liu, S.; Fu, Z.; Liu, S.; Zhao, Q. Jacobi elliptic function expansion method and periodic wave solutions of nonlinear wave equations. *Phys. Lett. A* **2006**, *289*, 69–74. [CrossRef]

40. Shen, S.; Pan, Z. A note on the Jacobi elliptic function expansion method. *Phys. Lett. A* **2003**, *308*, 143–148. [CrossRef]

41. Liu, G.T.; Fan, T.Y. New applications of developed Jacobi elliptic function expansion methods. *Phys. Lett. A* **2005**, *345*, 161–166. [CrossRef]

42. Islam, S.R.; Wang, H. Some analytical soliton solutions of the nonlinear evolution equations. *J. Ocean. Eng. Sci.* **2022**, *in press*. [CrossRef]

43. Wang, M.; Zhou, Y.; Li, Z. Application of a homogeneous balance method to exact solutions of nonlinear equations in mathematical physics. *Phys. Lett. A* **1996**, *216*, 67–75. [CrossRef]

44. Wang, Z.L.; Sun, L.J.; Hua, R.; Zhang, L.H.; Wang, H.F. Lie Symmetry Analysis, Particular Solutions and Conservation Laws of Benjiamin Ono Equation. *Symmetry* **2022**, *14*, 9. [CrossRef]

45. Huo, C.; Li, L. Lie Symmetry Analysis, Particular Solutions and Conservation Laws of a New Extended (3+1)-Dimensional Shallow Water Wave Equation. *Symmetry* **2022**, *14*, 1855. [CrossRef]

46. Akram, G.; Sadaf, M.; Zainab, I. The dynamical study of Biswas–Arshed equation via modified auxiliary equation method. *Optik* **2022**, *255*, 168614. [CrossRef]

47. Akram, G.; Sadaf, M.; Abbas, M.; Zainab, I.; Gillani, S.R. Efficient techniques for traveling wave solutions of time-fractional Zakharov–Kuznetsov equation. *Math. Comput. Simul.* **2022**, *193*, 607–622. [CrossRef]

48. Khater, M.M.; Lu, D.; Attia, R.A. Dispersive long wave of nonlinear fractional Wu-Zhang system via a modified auxiliary equation method. *AIP Adv.* **2019**, *9*, 25003. [CrossRef]

49. Khater, M.M.; Attia, R.A.; Lu, D. Modified auxiliary equation method versus three nonlinear fractional biological models in present explicit wave solutions. *Math. Comput. Appl.* **2018**, *24*, 1. [CrossRef]

50. Wang, X.; Ehsan, H.; Abbas, M.; Akram, G.; Sadaf, M.; Abdeljawad, T. Analytical solitary wave solutions of a time-fractional thin-film ferroelectric material equation involving beta-derivative using modified auxiliary equation method. *Results Phys.* **2023**, *48*, 106411. [CrossRef]
51. Mohammed, W.W.; Cesarano, C.; Al-Askar, F.M. Solutions to the (4+ 1)-Dimensional Time-Fractional Fokas Equation with M-Truncated Derivative. *Mathematics* **2022**, *11*, 194. [CrossRef]
52. Sousa, J.V.D.C.; de Oliveira, E.C. A new truncated *M*-fractional derivative type unifying some fractional derivative types with classical properties. *Int. J. Anal. Appl.* **2018**, *16*, 83–96.
53. Akram, G.; Arshed, S.; Sadaf, M.; Farooq, K. A study of variation in dynamical behavior of fractional complex Ginzburg-Landau model for different fractional operators. *Ain Shams Eng. J.* **2023**, *14*, 102120. [CrossRef]
54. Shahen, N.H.M.; Bashar, M.H.; Ali, M.S. Dynamical analysis of long-wave phenomena for the nonlinear conformable space-time fractional (2+ 1)-dimensional AKNS equation in water wave mechanics. *Heliyon* **2020**, *6*, e05276. [CrossRef]